PERFORMANCE ANALYSIS OF A FREE SPACE OPTICAL LINK WITH SPACE TIME BLOCK CODE

A thesis submitted in partial fulfilled of the requirements for the degree of

Master of Science
in
Electrical and Electronic Engineering

By
Md. Shariful Islam

Under the supervision of
Professor Dr. Satya Prasad Majumder

Department of Electrical and Electronic Engineering

Bangladesh University of Engineering and Technology

October 2012

The thesis entitled **"Performance Analysis of a Free Space Optical Link with Space Time Block Code"** submitted by Md. Shariful Islam, Roll no: 100606203P, Session: October 2006 has been accepted as satisfactory in partial fulfillment of the requirements for the degree of **Master of Science in Electrical and Electronic Engineering** on October 2012.

BOARD OF EXAMINERS

1. _____
(Dr. Satya Prasad Majumder) **Chairman**
Professor
Department of Electrical and Electronic Engineering
Bangladesh University of Engineering and Technology
Dhaka-1000

2. _____
Dr. Pran Kanai Saha
Professor and Head **(Ex-Officio)**
Department of Electrical and Electronic Engineering
Bangladesh University of Engineering and Technology
Dhaka-1000

3. _____
Dr. Mohammed Imamul Hassan Bhuiyan
Associate Professor **Member**
Department of Electrical and Electronic Engineering
Bangladesh University of Engineering and Technology
Dhaka-1000

4. _____
Engr. Md. Abdul Moqaddem
MBA, M.Sc. Engg.(EEE, BUET) **Member**
Director Telecom (DTR, West) **(External)**
Bangladesh Telecommunications Company Limited
Sher-e-Bangla Nagar, Dhaka-1207

Declaration

I hereby declare that this thesis has been done by me and it or any part of it has not been submitted elsewhere for any other degree or diploma.

Signature of the candidate

(Md. Shariful Islam)
Roll No.: 100606203P

Dedication

To my beloved wife (Rita) & daughter (Sara)

Acknowledgement

I am deeply grateful to my supervisor Prof. Dr. Satya Prasad Majumder for his consistent guidance, relentless encouragement, helpful suggestions, constructive criticism and endless patience throughout the progress of this research. The successful completion of this thesis would not been possible without persistent motivation and continuous guidance of my honorable supervisor. I wish to express my profound indebtedness and thanks to him for his advice throughout the entire course of this work.

I am also grateful to Dr. Pran Kanai Saha, Professor and Head, Department of Electrical and Electronic Engineering, Bangladesh University of Engineering and Technology (BUET), Dhaka, for providing valuable suggestions on writing a satisfactory thesis.

I, also express my profound indebtedness to all my teachers for their continuous encouragement and providing me their helping hand whenever required.

I am also indebted to my family members for their encouragement and patience.

Contents

List of Abbreviations

APD	**Avalanche photodiode**
AWGN	**Additive white gaussian noise**
BER	**Bit error rate**
EGC	**Equal gain combiner**
FOV	**Field of view**
FSO	**Free-space optical**
IM/DD	**Intensity modulation direct detection**
LED	**Light emitting diode**
MIMO	**Multiple input Multiple output**
MISO	**Multiple input single output**
MLMD	**Multi laser multi detector**
MLCD	**Mars laser communication demonstration**
MRC	**Maximal ratio combining**
NEC	**Nippon electric company**
OFC	**Optical fiber cable**
OBPF	**Optical band pass filter**
OOK	**On-off keying**
PSD	**Power spectral density**
p.d.f	**Probability of density function**
PPM	**Pulse position Modulation**
RF	**Radio frequency**
SI	**Scintillation index**
SISO	**Single input single output**
SIMO	**Single input multiple output**
SNR	**Signal to noise ratio**
STBC	**Space time block code**
SelC	**Selection combiner**
WDM	**Wavelength division multiplexing**

List of Tables

List of Figures

Abstract

With the worldwide demand for larger bandwidth and greater mobility there is a rapid advancement in the area of broadband wireless communications. The high capacity and low loss of optical fiber has seen its exploding growth in the last few decades in the WANs and LANs. Free space optical (FSO) wireless communication has emerged as a viable technology for bridging the gap in existing high data rate fiber network and as a temporary backbone for rapidly deployable mobile wireless communication infrastructure. We believe that FSO will be one of the most unique and powerful tools to address connectivity bottlenecks that have been created in high-speed networks during the past decade due to the tremendous success and continued acceptance of the Internet. However, optical wave propagation through the air experiences fluctuation in amplitude and phase due to atmospheric turbulence. The intensity fluctuation, also known as scintillation is one of the most important factors that degrade the performance of an FSO communication link even under the clear sky condition. FSO systems offer capacities in the range of 100Mbps to 2.5 Gbps, and data rates as high as 160 Gbps, enabling optical transmission up to 2.5 Gbps of data, voice, and video communications through the air, thus allowing optical connectivity without deploying fiber optic cables or securing spectrum licenses.

In this thesis, the performance of an FSO link using Alamouti-type Space Time Block Code (STBC) over log-normal atmospheric turbulence-induced fading channels has been investigated. Based on the modification of the Alamouti code presented by Simon and Vilnrotter, a generalized approach is adopted to consider space-time coded on-off keying (OOK) formats for improvement the Bit Error Rate (BER) performance. It is shown that the deployment of modified space-time coding is necessary for a FSO IM/DD link. The added diversity contributes a significant improvement in BER performance.

Chapter 1

Introduction

Chapter-1

Introduction

1.1 Background

Free-space optical communication (FSO) is an age long technology that entails the transmission of information laden optical radiation through the atmosphere from one point to the other. Around 800 BC, ancients Greeks and Romans used fire beacons for signaling and by 150 BC the American Indians were using smoke signals for the same purpose of signaling. Other optical signaling techniques such as the semaphore were used by the French sea navigators in the 1790s; but what can be termed the first optical communication in an unguided channel was the Photophone experiment by Alexander Graham Bell in 1880 [1, 2]. In his experiment, Bell modulated the Sun radiation with voice signal and transmitted it over a distance of about 200 metres. The receiver was made of a parabolic mirror with a selenium cell at its focal point. However, the experiment did not go very well because of the crudity of the devices used and the intermittent nature of the sun radiation.

The fortune of FSO changed in the 1960s with the discovery of optical sources, most importantly, the laser. A flurry of FSO demonstrations was recorded in the early 1960s into 1970s. Some of these included the: spectacular transmission of television signal over a 30 mile (48 km) distance using a GaAs light emitting diode by researchers working in the MIT Lincolns Laboratory in 1962 [3]; a record 118 miles (190 km) transmission of voice modulated He-Ne laser between Panamint Ridge and San Gabriel Mountain, USA in May 1963 [3]; and the first TV-over-laser demonstration in March 1963 by a group of researchers working in the North American Aviation [3]. The first laser link to handle commercial traffic was built in Japan by the Nippon Electric Company (NEC) around 1970. The link was a full duplex 0.6328 μm He-Ne laser FSO between Yokohama and Tamagawa, a distance of 14 km [3].

From this time on, FSO has continued to be researched and used chiefly by the military for covert communications. FSO has also been heavily researched for deep space applications by NASA and ESA with programs such as the then Mars Laser Communication Demonstration (MLCD) and the Semiconductor-laser Inter-satellite Link Experiment (SILEX) respectively [4]. In spite of early knowledge of the necessary techniques to build an operational laser communication system, the usefulness and practicality of a laser communication system was until recently questionable for many reasons [3]. First, existing communications systems were adequate to handle the demands of the time. Second, considerable research and development were required to improve the reliability of components to assure reliable system operation. Third, a system in the atmosphere would always be subject to interruption in the presence of heavy fog. Fourth, use of the system in space where atmospheric effects could be neglected required accurate pointing and tracking optical systems which were not then available. In view of these problems, it is not surprising that until now, FSO had to endure a slow penetration into the access network.

With the rapid development and maturity of optoelectronic devices, FSO has now witnessed a re-birth. Several successful field trials have been recorded in the last few years in various parts of the world which have further encouraged investments in the field [5]. This has now culminated into the increased commercialization and the deployment of FSO in today's communication infrastructures.

FSO has now emerged as a commercially viable complementary technology to radio frequency (RF) and millimeter wave wireless systems for reliable and rapid deployment of data, voice and video within the access networks. RF and millimeter wave based wireless networks can offer data rates from tens of Mbps (point-to-multipoint) up to several hundred Mbps (point-to-point). However, there is a limitation to their market penetration due to spectrum congestion, licensing issues and interference from unlicensed bands. The future emerging license-free bands are promising, but still have certain bandwidth and range limitations compared to the FSO. The short-range FSO links are used as an alternative to the RF links for the last or first mile to provide broadband access network to homes and offices as well as a high bandwidth bridge between the local and wide area networks. Full duplex FSO systems running at 1.25 Gbps between two static nodes are now common sights in today's market just like FSO systems that

operate reliably in all weather conditions over a range of up to 3.5 km. In 2008, the first 10 Gbps FSO system was introduced to the market, making it the highest-speed commercially available wireless technology [6]. Efforts are continuing to further increase the capacity via integrated FSO/fibre communication systems and wavelength division multiplexed (WDM) FSO systems which are currently at experimental stages.

The earlier skepticism about FSO‟s efficacy, its shrinking acceptability by service providers and slow market penetration that hampered continuously it in the 1980s are now rapidly fading away judging by the number of service providers, organizations, government and private establishments that now incorporate FSO into their network infrastructure [5]. Terrestrial FSO has now proven to be a viable complementary technology in addressing the contemporary communication challenges, most especially the bandwidth/high data rate requirements of end users at an affordable cost. The fact that FSO is transparent to traffic type and data protocol makes its integration into the existing access network far more rapid. Nonetheless, the atmospheric channel effects such as thick fog, smoke and turbulence as well as the attainment of 99.999% availability still pose the greatest challenges to long range terrestrial FSO.

1.2 Types of Optical Communication

1.2.1 Fiber Optic Communication System

Fiber-optic communication is a technique of transmitting information from one place to another by sending pulses of light through an optical fiber. An optical fiber is a thin, flexible, transparent fiber that works as a waveguide, or "light pipe", to pass on light between the two ends of the fiber. Optical fiber typically consists of a crystal clear core surrounded by a transparent cladding material with a lower index of refraction. Light is kept in the core by total internal reflection. This causes the fiber to act as a waveguide. The light forms an electromagnetic carrier wave that is modulated to bring information. The developments of low loss optical fiber (1970's) have revolutionized fiber-optic communication systems in the telecommunications industry and have played most important role in the advent of the Information Age. Because of its advantages over

electrical transmission, optical fibers have largely replaced copper wire communications in core networks in the developed world.

1.2.2 Free Space Optical Communication

FSO uses infrared lasers for transmitting optical signals through the air. Also known as "wireless optics," FSO provides point-to-point and point-to-multipoint transmission at very high speeds without requiring a government license for use of the spectrum. FSO requires line of sight. Because weather conditions such as fog can reflect light signals, redundant paths can be created by sending multiple signals to reflectors on different buildings. Transmitters with multiple beams are also used to provide greater reliability.

Advantages of the FSO

i. Ease of deployment
ii. License-free long-range operation
iii. High bit rates
iv. Low bit error rates
v. Immunity to electromagnetic interference
vi. Full duplex operation
vii. Very secure due to the high directionality and narrowness of the beam(s)

Drawbacks of the FSO

i. Pointing error due to building sway
ii. Intensity fluctuation which is also known as scintillation is one of the most important factors that degrade the performance of a MIMO FSO communication link even under the clear sky condition
iii. Atmospheric turbulence has strong effect on MIMO wireless system

1.3 Review of Previous Works on FSO Links

In reference [7] & [8], it is found that the performance of the free space optical systems can be severely limited by optical crosstalk, misalignments between the transmitter and receiver.

In addition atmospheric turbulence causes fluctuations in both the intensity and phase of the received light signal which results in impairments of the link performance [9][10]. FSO communication is less affected by snow and rain, but severely affected by the atmospheric turbulence and fog [9][11].

In reference [10]-[12], it is found that two primary challenges for FSO communication are pointing error and fading due to scattering and scintillation.

The performance of an FSO link considering Alamouti-type STBC over strong atmospheric turbulence has been reported in reference [13].

Free space laser communication systems based on a single laser source and single detector suffers the effect of atmospheric turbulence much [10][12]. The communication system based on the use of a Multiple Laser Multiple Detector (MLMD) architecture can considerably diminish the effect of this problem [7][8][10].

Already different modulation schemes are examined for the FSO system through atmospheric turbulence [9]-[12].

Several research works are reported on FSO link performance considering the above limitation [11][15]. Improvement in the performance of an FSO link using receive antenna diversity is also reported recently [12][14]. Further research works are also reported on FSO system with Multiple Input Multiple Output (MIMO) configurations of transmit and receive antennas including the effect of strong turbulence [11][13][15].

1.4 Objective with Specific Aims and Possible Outcome

The main objective of this thesis is to analyze the performance of a MIMO optical free space link considering weak turbulence and with the application of the Alamouti-type space time block codes and different receive combining techniques such as MRC, Selection Combining etc. The main objectives of this thesis are—

a. To carry out analysis to find the expression of the received optical signal considering FSO link with weak turbulence and the expression of the conditional signal to noise ratio

(SNR) conditioned on a given value of turbulence for multiple transmit and multiple receive antennas considering MRC and Selection combining technique.

b. To extend the analysis to find the conditional and the average Bit Error Rate of the MIMO optical system with Alamouti type space time block codes with different transmitter and receiver diversity combinations.

c. To find the BER performance results and the improvements in system performance due to space time block coding and to compare with the coding gains over those for strong turbulence at a given system BER and to determine the optimum system design parameters.

1.5 Outline of Methodology/ Experimental Design

Considering multiple transmitter with space time block codes of different formats, expression will be developed for the transmitted and received optical fields at the output of a PIN photo detector. Maximal ratio and Selection combining techniques will be used to find the output current of the combiner. The expression for the signal current and noise currents will be developed considering channel impairments like turbulence, fading and scattering of the optical signal. The probability density function (pdf) of the output signal will also be developed for the above combining techniques. The BER, conditioned on a given value of turbulence will be developed and the average BER expression will be derived by averaging the conditional BER over the pdf of the output signal. The expression for the output Signal to Noise ratio (SNR) and BER will be derived for different number of transmit and receive antennas. The performance results will be evaluated numerically. Also the improvement in system performance over IM/DD system and optimum design parameters will be found. Comparison of results with strong turbulence will also be carried out.

1.6 Organization of this Thesis

Chapter 1 is concentrated on the purpose and present state of FSO communication system and importance of FSO communication. A brief overview of the different components of the FSO

communication system and the impact of atmospheric condition on FSO communication link is discussed in Chapter 2. Chapter 3 is provided with the techniques and technological details of Alamouti type STBC with MIMO through atmospheric turbulence channel. Numerical results are presented in Chapter 4 to point out the performance under different receiver combining schemes such as MRC and Selection combining technique etc. Finally, concluding remarks and some proposals for future work are given in Chapter 5.

Chapter 2

Review of Free Space Optical Communications

Chapter-2

Review of Free Space Optical Communications

2.1 Introduction

The ultimate goal of the optical signal transmission is to achieve the predetermined bit error rate (BER) between any two nodes in an optical network. The optical transmission system has to be properly designed to provide reliable operation during its lifetime, which includes the management of key engineering parameters.

FSO uses a directed beam of light radiation between two end points to transfer information (data, voice or even video) which is similar to OFC (optical fiber cable) networks where light pulses are sent through free air instead of OFC cores. Depending upon the atmospheric condition the transmitted optical beam passing through the atmosphere can be absorbed, scattered or displaced. The key optical components used in the FSO communication are discussed in this chapter along with different FSO systems under different atmospheric turbulence conditions.

2.2 Block Diagram of FSO Communication System

A free space optical links consists of a transmitter, FSO communication channels and a receiver as shown in Fig. 2.1.

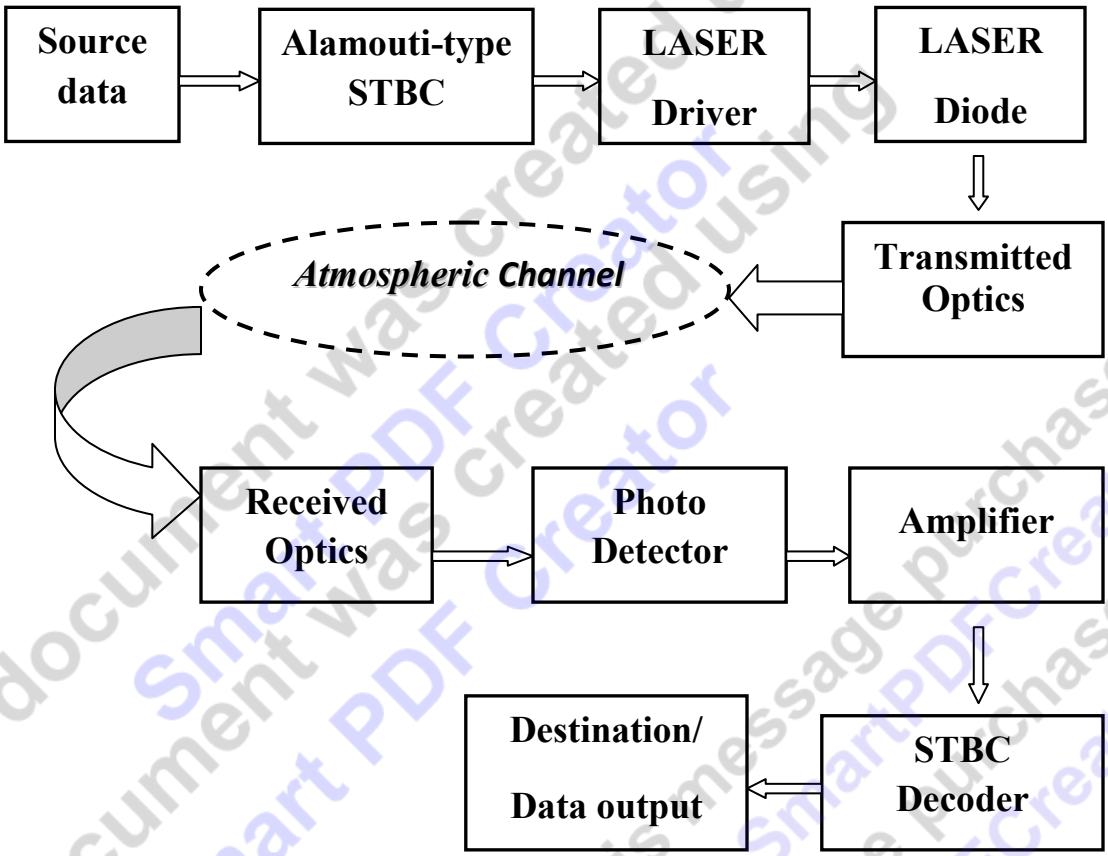

Fig. 2.1: FSO MIMO system block diagram

2.2.1 Transmitters

Semiconductor lasers and light emitting diodes (LED) are currently used as the primary transmission media in commercial FSO systems. These transmission sources differ according to their wavelength, power, and modulation speed. Normally specific transmission source is

designed for a specific application. Electroluminescent diodes and semiconductor junction lasers have a great advantage since their radiant powers and optical frequencies can be directly modulated by the injection current. Modulation frequencies up to several tens of GHz can be reached; these performances depend on the material and the internal structure of the components.

Light Emitting Diodes

Light Emitting Diodes are widely used today because of emission of fairly narrow bandwidth of either visible light at different colored wavelengths invisible infra-red light for remote controls or laser type light when a forward current is passed through them. They are basically PN junction diodes, made from a very thin layer of fairly heavily doped semiconductor material. When the diode is forward biased, electrons from the semiconductors conduction band recombine with holes from the valence band releasing sufficient energy to produce photons which emit a monochromatic light. Because of this thin layer a reasonable number of these photons can leave the junction and radiate away producing a colored light output.

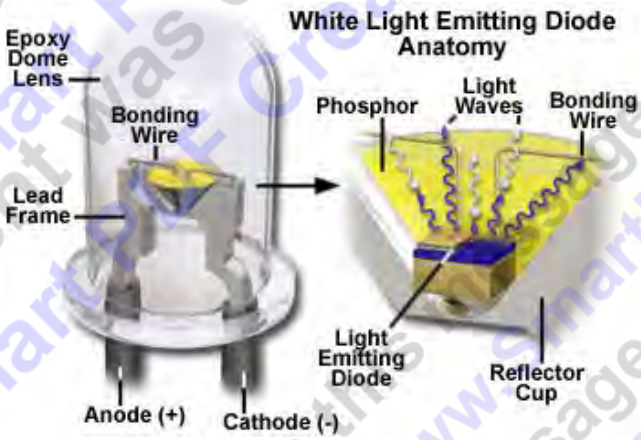

Fig. 2.2: LED construction [16]

LEDs are current-dependent devices with its forward voltage drop V_F, depending on the semiconductor compound (its light color) and on the forward biased LED current. The point where conduction begins and light is produced is about 1.2V for a standard red LED to about 3.6V for a blue LED. The voltage drop across the LED at a particular current value, for example 20mA, will also depend on the initial conduction V_F point. As an LED is effectively a diode, its

forward current to voltage characteristics curves can be plotted for each diode color as shown in Fig 2.3 [16].

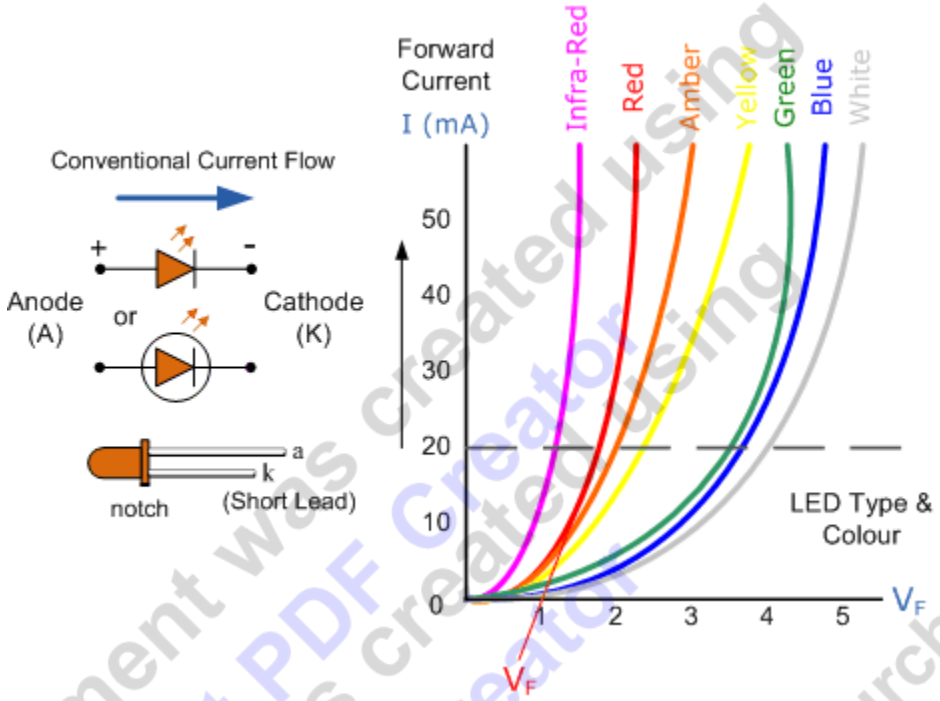

Fig. 2.3: LED and its I-V characteristics

Lasers

Lasers are devices that produce intense beams of light which are monochromatic, coherent, and highly collimated. The wavelength of laser light is extremely monochromatic when compared to other sources of light, and all of the photons energy that make up the laser beam have a fixed coherence with respect to one another. Light from a laser typically has very low divergence. It can travel over great distances or can be focused to a very small spot with a brightness which exceeds that of the sun.

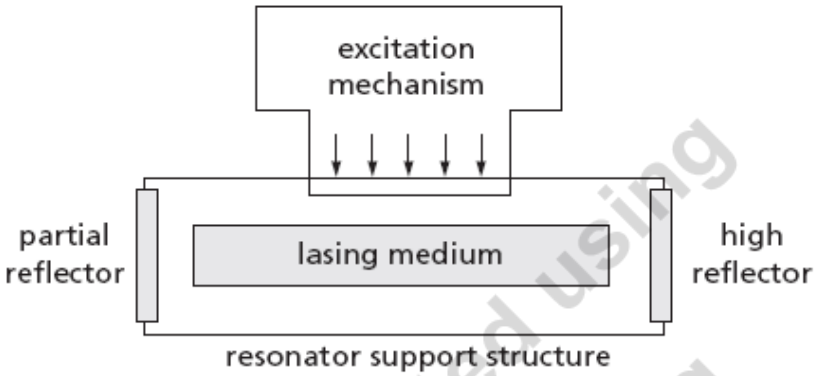

Fig. 2.4: Schematic diagram of a basic laser [17]

The two most important basic principles for laser science are the quantum nature of light and a process called stimulated emission. The quantum nature of light refers to light quantized into discrete energy portions, nowadays called photons.

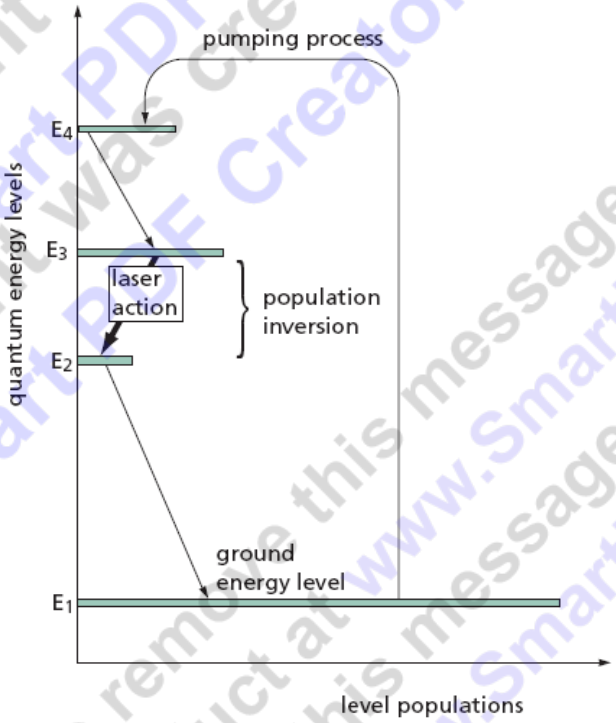

Fig. 2.5: A four-level laser pumping system [17]

A laser basically consists of three parts: a resonant optical cavity called the optical resonator, a laser gain medium (also called active laser medium) and a pump source to excite the particles in the gain medium. The active particles in the laser gain medium need to be in a state of inversion

for the laser to operate. To reach this state requires some pumping process, which lifts them into the required energy state.

2.2.2 Receivers

When the transmitted light passes through the atmosphere, it must be collected by the receiver. The received light from the air is firstly converted into electrical signal by the photo detector. Then it is amplified and is passed through the ML-decoder. Two popular photo detectors are p-i-n photodiode and avalanche photodiode. A brief description is given below-

P-i-N Photodiodes

A P-i-N diode is a type of diode that contains a semiconductor with a very large intrinsic region between a smaller-than-normal p-type and n-type region. A P-i-N diode is used for three basic reasons: as a radio frequency (RF) switch, as part of a photovoltaic cell and as an emergency shunt for power overloads.

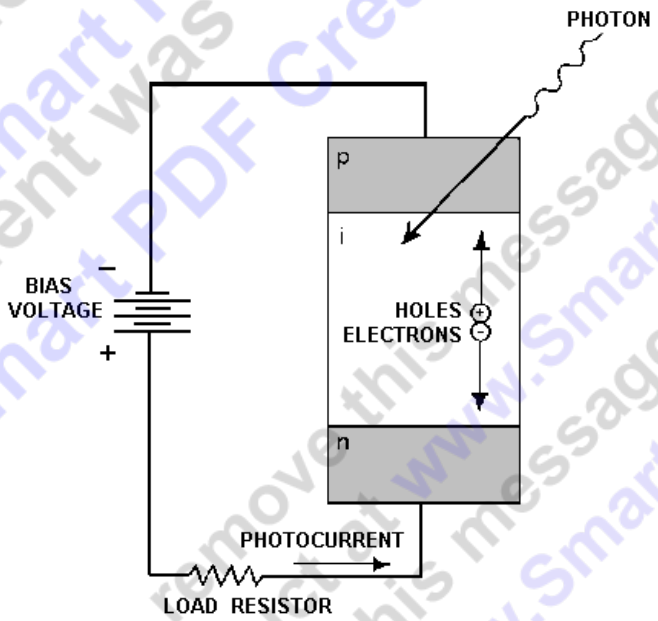

Fig. 2.6: A simple P-i-N photodiode circuit [17]

When a P-i-N diode is forward biased, the injected carrier concentration is typically several orders of magnitude higher than the intrinsic level carrier concentration. Because of this high level injection, the electric field extends deeply (almost the entire length) into the region. This

electric field helps in speeding up of the transport of charge carriers from P to N region, resulting in faster operation of the diode, which makes it a suitable device for high frequency operations.

Avalanche Photodiodes

Avalanche photodiodes (APD) are very popular semiconductor detectors. The avalanche photodiode (APD) is different from the PIN photodetector in that it provides an inherent current gain through the process called repeated electron ionization. This culminates in increased sensitivity since the photocurrent is now multiplied before encountering the thermal noise associated with the receiver circuit. Hence the expression for the responsivity of an APD includes a multiplication (or gain) factor g. Typical gain values lie in the range 50 to 300 [18], thus the responsivity value of an APD can be greater than unity. Fig 2.7 shows the internal structure of an APD.

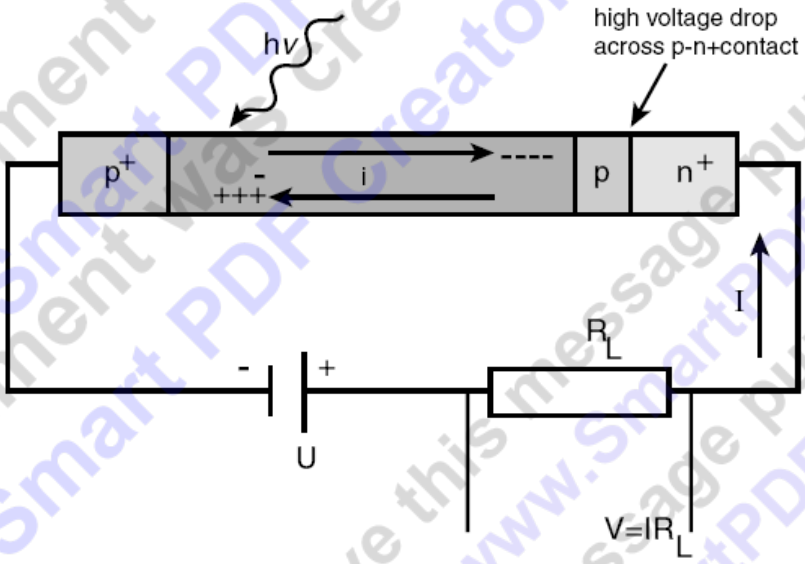

Fig. 2.7: Schematics of a reach-through APD structure [19]

The APD offers a higher sensitivity than the PIN detector but the statistical nature of the ionization/avalanche process means that there is always a multiplication noise associated with the APD. The avalanche process is also very temperature-sensitive. These factors are very important and must always be taken into account whenever an APD is used in an optical communication system.

2.3 FSO Transmission Channel

FSO links contain the transmission, absorption and scattering of light by the atmosphere. Under normal conditions, the atmosphere has variety of different molecules and small suspended particles (aerosols) which interacts with light. This interaction produces a wide variety of optical phenomena such as selective attenuation of radiation, absorption at specific optical wavelengths due to the molecules, scattering due to the sky blue color, the red sunset, radiative emission of an optical beam etc., and scintillation due to the variation of the air's refractive index under the effect of temperature (stars twinkle).

The performance of any optronic system depends not only on its intrinsic design features resulting from its design and the technology used, but also on its behavior in its operational environment. However, the construction of such a system, made up of a transmitter and a receiver in free atmosphere, necessitates proper knowledge of specific optical properties of the atmosphere. Scattering and absorption of the radiation from the medium affect spectral transmission of the propagation medium. Therefore, it is useful to know how optronic systems behave in differing climatic and weather conditions and particularly under prevailing environmental conditions.

Absorption primarily happens by the gasses for energy traveling through the atmosphere which results atmospheric attenuation. For lower frequencies (below 10 GHz), the attenuation is reasonably predictable. For high frequencies in the millimeter wave range, the attenuation not only increases, but becomes more dependent upon peculiar absorbing characteristics of H_2O, O_2, and the like.

Scattering is the process by which "small particles suspended in a medium of a different index of refraction diffuse a portion of the incident radiation in all directions." With scattering, there is no energy transformation, but a change in the spatial distribution of the energy. This diffuses the light-- spreading it out in all directions so it is not just a single, straight beam. If it was not for scattering, we would not be able to see shadowed objects such as walnuts that have fallen on the ground under the shading of a tree [20].

Atmospheric aerosols are extremely fine particles (solid or liquid) suspended in the atmosphere with a very low fall speed caused by gravity. Aerosols may cause severe disturbance to the

propagation of optical and infrared waves, since their dimensions are very close to the wavelengths of these frequencies. But in case of centimeter and millimeter waves, the wavelength is much longer than the size of the aerosols. The most harmful environmental conditions are fog and haze due to their high concentration of scattering particles though rain and snow can hamper light propagation.

However, it is clear from the aforementioned discussion that the transmitted optical beam passing through the atmosphere can be absorbed, scattered or displaced depending on the atmospheric condition. This is the fundamental limits of FSO systems. FSO is less affected by snow and rain, but can be severely affected by the atmospheric turbulence and fog with compared to the RF system [21].

2.4 The Atmospheric Turbulence Models

In homogeneities caused by turbulence can be viewed as discrete cells, or eddies of different temperature, acting like refractive prisms of different sizes and indices of refraction. The interaction between the laser beam and the turbulent medium results in random phase and amplitude variations (scintillation) of the information-bearing optical beam which ultimately results in performance degradation of FSO links.

Atmospheric turbulence results in random fluctuation of the atmospheric refractive index, n along the path of the optical field/radiation traversing the atmosphere. This refractive index fluctuation is the direct end product of random variations in atmospheric temperature from point to point [22]. These random temperature changes are a function of the atmospheric pressure, altitude and wind speed. The smallest and the largest of the turbulence eddies are termed the inner scale, l_0, and the outer scale, L_0, of turbulence respectively. l_0 is typically on the order of a few millimetres while L_0 is typically on the order of several meters [11][23]. These weak lens-like eddies shown graphically in Fig. 2.8 result in a randomised interference effect between different regions of the propagating beam causing the wavefront to be distorted in the process.

The relationship between the temperature of the atmosphere and its refractive index is given by (4.1) [24].

$$\eta = 1 + 77.6(1 + 7.52 \times 10^{-3} \lambda^{-2}) \frac{P}{T_e} \times 10^{-6} \quad (2.1)$$

where P is the atmospheric pressure in millibars, T_e is the temperature in Kelvin and λ is the wavelength in microns.

Generally three types of atmospheric turbulence models are used.

a) Log Normal Distribution

b) Gamma-Gamma Model and

c) Negative Exponential Model

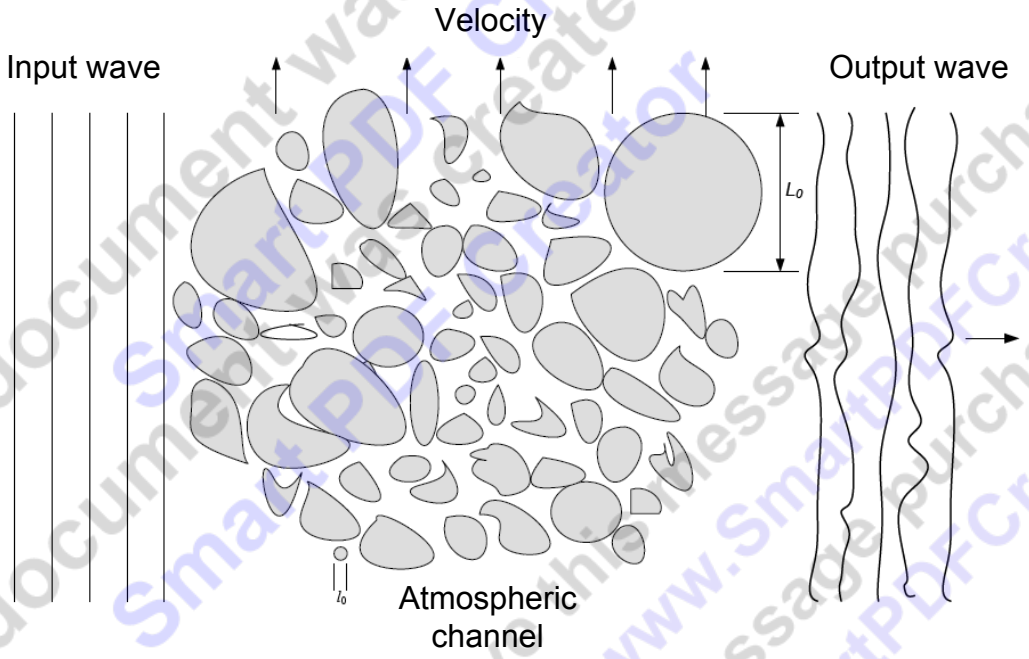

Fig. 2.8: Atmospheric channel with turbulent eddies [21]

2.4.1 Log- normal Distribution

The atmospheric turbulence impairs the performance of an FSO link by causing the received optical signal to vary randomly thus giving rise to signal fading. The fading strength depends on the link length, the wavelength of the optical radiation and the refractive index structure parameter C_n^2 of the channel. The log-normal distribution is generally used to model the fading associated with the weak atmospheric turbulence regime. This model is mathematically tractable

and it is characterized by the Ryotov variance σ_X^2. The turbulence induced fading is termed weak when σ_X^2<1.2 and this defines the limit of validity of the log-normal model. Beyond the weak turbulence regime, other models such as the gamma-gamma and the negative exponential will have to be considered. The Ryotov variance σ_X^2 can be calculated as

$$\sigma_X^2 = 1.23 C_n^2 (\sqrt[6]{k^7 L^{11}}) \tag{2.2}$$

where L is the propagation distance and k is the wave number.

The amplitude of the random path gain, $H = e^X$, where X is normal with mean μ_X and variance σ_X^2. Thus, the logarithm of the field amplitude scale factor is normally distributed. The optical intensity $I = H^2$ is also log normally distributed and the mean path intensity is unity, i.e., $E[H^2] = 1$, in this case [10]. The probability density function for H is-

$$f_H(a) = \frac{1}{(2\pi\sigma_X^2)^{0.5} a} \exp\left(-\frac{(\log_e a - \mu_x)^2}{2\sigma_X^2}\right), \quad a > 1 \tag{2.3}$$

Fig. 2.9 shows the lognormal distribution of intensity fluctuation with different scintillation index. The normalized variance of intensity which characterizes the strength of irradiance fluctuation is often referred to as the scintillation index. The scintillation index (S.I.) increases linearly with the Rytov parameter within the weak atmospheric regime.

For the log-normal distribution, the scintillation index, defined as

$$S.I. = \frac{E[H^4]}{E^2[H^2]} - 1 \tag{2.4}$$

This index can be related to the parameter σ_X^2 by S.I. = $e^{4\sigma_X^2} - 1$.Typical values appearing in the literature for S.I. are in the range 0.4–1.0.

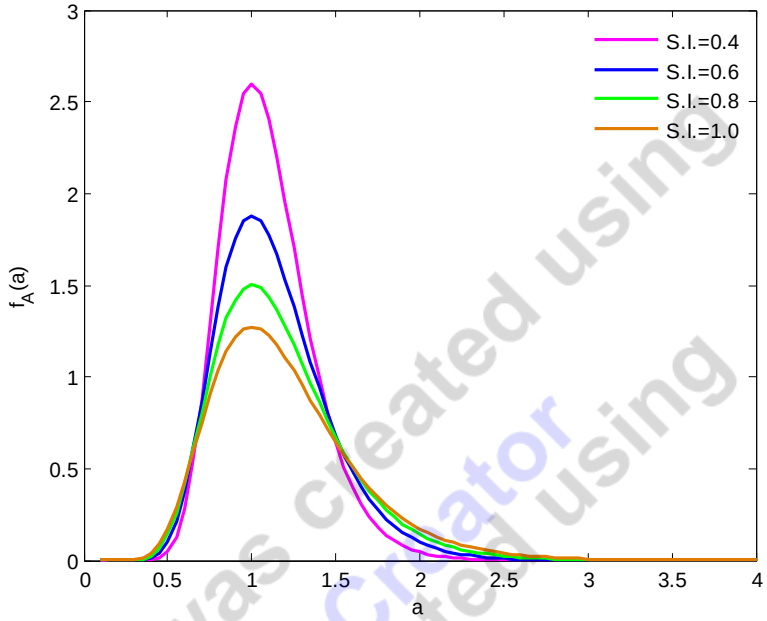

Fig. 2.9: Lognormal distribution of intensity fluctuation with different *S.I.*

2.4.2 Gamma-Gamma Model

For a wide range of turbulence conditions (weak to strong) the fading gain *I* in FSO systems can be modeled by a Gamma–Gamma distribution [25]

$$P(I) = \frac{2(\alpha\beta)^{(\alpha+\beta)/2}}{\Gamma(\alpha)\Gamma(\beta)} I^{(\alpha+\beta)/2-1} K_{\alpha-\beta}(2\sqrt{\alpha\beta I}) \tag{2.5}$$

where parameters $\alpha > 0$ and $\beta > 0$ are linked to the so–called scintillation index $S.I. \equiv 1/\alpha+1/\beta+1/(\alpha\beta)$. α and β can be adjusted to achieve a good agreement between $P(I)$ and measurement data . Fig. 2.10 shows the Gamma – gamma distribution of intensity fluctuation with different α, β. This two parameters α and β that characterize the irradiance fluctuation probability density function are related to the atmospheric conditions. Alternatively, assuming spherical wave propagation, α and β can be directly linked to physical parameters via

$$\alpha = \left[\exp\left(\frac{0.49\chi^2}{(1+0.18d^2+0.56\chi^{12/5})^{7/6}} \right) - 1 \right]^{-1} \tag{2.6}$$

$$\beta = \left[\exp\left(\frac{0.51\chi^2(1+0.69\chi^{12/5})^{-5/6}}{(1+0.9d^2+0.62d^2\chi^{12/5})^{5/6}} \right) - 1 \right]^{-1} \tag{2.7}$$

where $\chi^2 = 0.5C_n^2 k^{7/6} L^{11/6}$, $d = (kD^2 / 4L)^{1/2}$, $C_n^2 = 5 \times 10^{-13} m^{-2/3}$ and $k=2\pi/\lambda$. Here, λ, D, C_n^2 and L are the wavelength in meters, the diameter of the receiver's aperture in meters, the index of refraction structure parameter, and the link distance in meters, respectively.

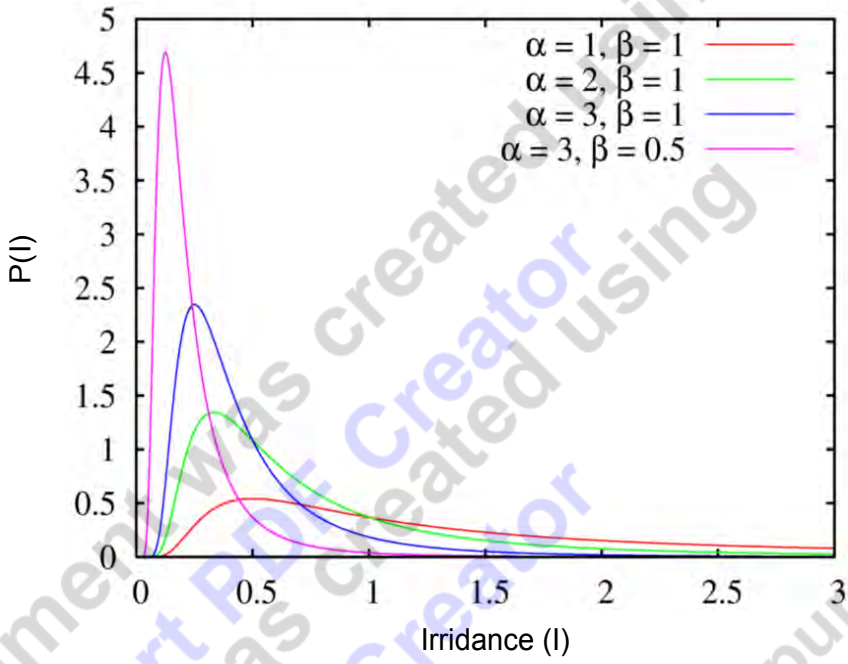

Fig. 2.10: Gamma - gamma distribution of intensity fluctuation with different *α, β*.

The probability density function of irradiance fluctuation of the Gamma-Gamma model is valid for all turbulence scenarios from weak to strong.

2.4.3 Negative Exponential Model

Negative exponential channel is generally considered under strong irradiance fluctuations where the link length spans several kilometres. The amplitude fluctuation of the field traversing the turbulent medium in this situation is experimentally verified to obey the Rayleigh distribution implying negative exponential statistics for the irradiance. The negative exponential pdf is as follows—

$$P(I) = \frac{1}{I_0} \exp(-\frac{I}{I_0}) \tag{2.8}$$

where, $I_0 > 0$.

I_0 is said as the mean irradiance or noise turbulence variance which is often normalized to unity. Fig. 2.11 shows the Negative exponential distribution of intensity fluctuation with different mean irradiance. This saturation regime is also called the fully developed speckle regime. During the saturation regime, the value of the scintillation index, $S.I. \rightarrow 1$.

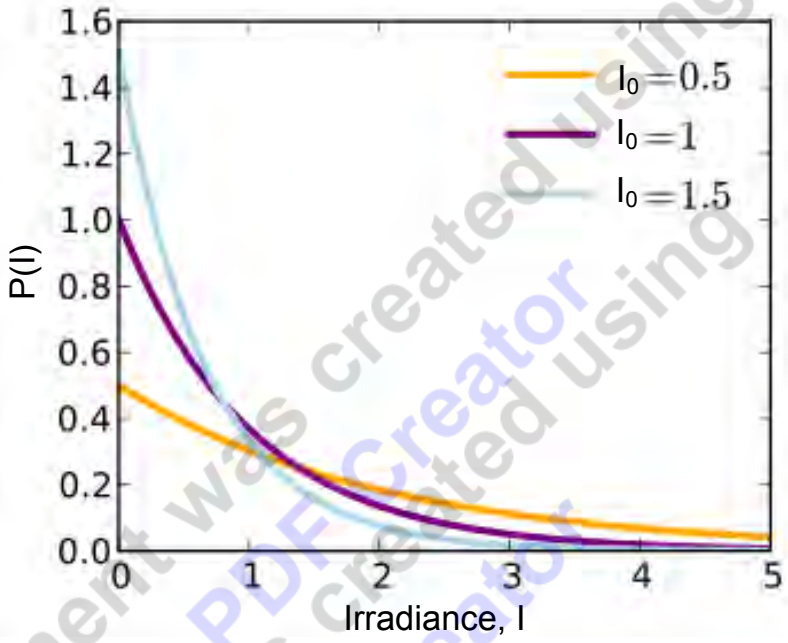

Fig. 2.11: Negative exponential distribution of intensity fluctuation with different I_0.

2.5 FSO with MIMO

To mitigate the deleterious effects of scattering and turbulence, multiple transmitters and receivers can be used. Hence, it would be possible to benefit from spatial diversity and receive multiple independent copies of the same signal. The effectiveness of Multiple-Input Multiple-Output (MIMO) systems in combating the log-normal amplitude fading and phase-front distortion have been demonstrated in the published literatures [26].

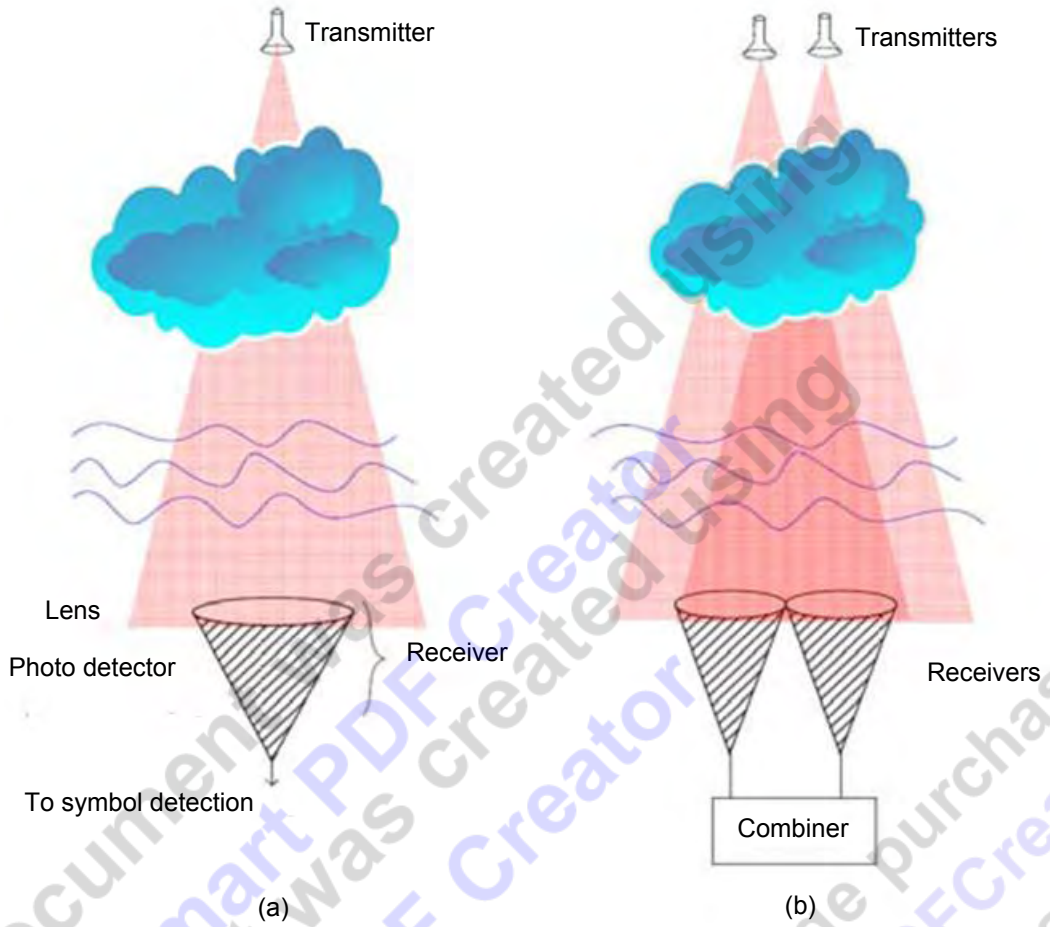

Fig. 2.12: (a) SISO and (b) MIMO communications systems.

Fig. 2.12(a) shows a Single-Input Single-Output (SISO) system operating in presence of clouds and turbulence. In fig. 2.12(b), the SISO system is replaced by a 2×2 MIMO system. Sum of the areas of smaller multiple receiving apertures is equal to the area of single aperture receiver. Moreover, total transmitted power is the same for SISO and MIMO transmitters. A single photo-detector is used in the focal plane of each receiving aperture, to ensure that in background noise-limited reception, the total collected noise is the same for both systems. As a result, transmitters and receivers should be placed such that, in turbulence-free conditions, a single photo-detector in the focal plane of each receiver can collect the signals from all transmitters.

The outputs of multiple receivers can be combined using either Equal Gain Combining (EGC), Selection Combining (SC) or Maximal Ratio Combining (MRC). Replacing the single high

power transmitter with multiple transmitters of the same total power may increase the system diversity order and hence is expected to improve the performance.

The combiner in MIMO system can be EGC, SC or MRC. SISO transmitter and receiver can be replaced by an arbitrary number of sub-apertures, and as long as the total transmitted power and area of receivers are kept the same, comparison of two systems is fair.

2.6 Diversity-Combining Techniques

Most common techniques for combining diversity signals are selection, feedback, maximal ratio, and equal gain.

In **maximal-ratio combining**, the signals from all of the branches are weighted according to their individual SNRs and then summed. The individual signals must be co-phased before being summed. The maximal-ratio combining can produce an acceptable average SNR. It uses each of the branches in a co-phased and weighted manner such that the largest possible SNR is available at the receiver.

Selection combining used in spatial diversity systems involves the sampling of antenna signals, and sending the largest one to the demodulator. Selection-diversity combining is relatively easy to implement but not optimal because it does not make use of all the received signals simultaneously.

Equal-gain combining is similar to maximal-ratio combining except that the weights are all set to unity. The possibility of achieving an acceptable output SNR from a number of unacceptable inputs is still retained. The performance is marginally inferior to maximal ratio combining.

With feedback or scanning diversity, the signals are scanned in a fixed sequence until one is found that exceeds a given threshold. This one becomes the chosen signal until it falls below the established threshold, and the scanning process starts again. The error performance of this technique is somewhat inferior to the other methods, but feedback is quite simple to implement.

2.6.1 Maximal-ratio combining

MRC takes better advantage of the diversity provided by all branches. In MRC the elements are weighted with their instantaneous SNRs. The branches are co-phased to get maximum advantage of diversity combining before the summation process. This summed signal is used for the decoding process which is shown in fig. 2.13. The performance of MRC is much better than that of the selection combining. However it is more complex since it requires SNR estimation and weight updates.

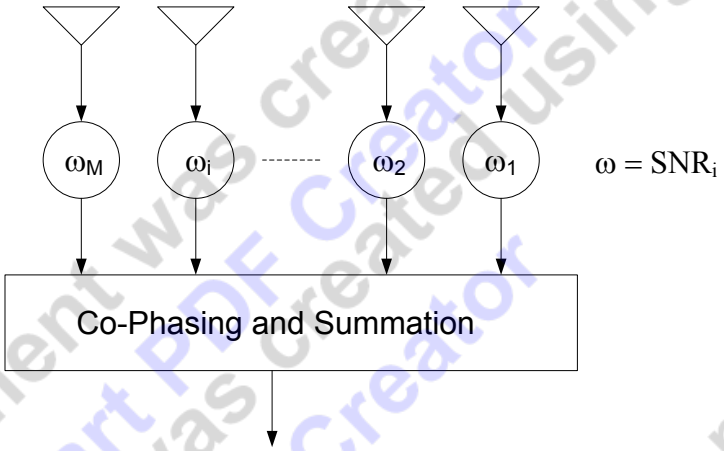

Fig. 2.13 Maximal ratio combining.

Maximal ratio combining represents a theoretically optimal combiner over fading channels as a diversity scheme in a communication system. Theoretically, multiple copies of the same information signal are combined so as to maximize the instantaneous SNR at the output.

Let us consider the operation of a pre-detection L-branch maximal ratio combiner (MRC) on correlated Rayleigh fading channels. The received signals are assumed to be corrupted by additive white Gaussian noise (AWGN). The combiner input from the ℓ-th channel, $\ell = 1 \ldots L$ is given by

$$y_\ell(t) = g_\ell(t)u(t) + n_\ell(t) \tag{2.9}$$

where $g_\ell(t)$ is the complex Gaussian channel gain, $u(t)$ is the transmitted information signal and $n_\ell(t)$ is the noise. If we assume that the spatial correlation between two received signals from any two of the combiner inputs from antennas located at positions x_k and x_ℓ following from [27] is

$$\rho(x_k, x_\ell) = \frac{E\{g_k(t)g_\ell^*(t)\}}{\sqrt{E\{g_k(t)g_k^*(t)\}E\{g_\ell(t)g_\ell^*(t)\}}} \tag{2.10}$$

where $(\cdot)^*$ denotes the conjugate, and $E\{\cdot\}$ denotes the mathematical expectation. The time index t will be discarded from this point because only spatial correlation is being considered and a quasi-static analysis is being applied.

2.6.2 Selection combining

In selection combining, the branch with the largest SNR is selected and that element's signal is used for the decoding process. Compared with other two schemes, selective diversity is much easier to implement without much performance degradation, especially for the reverse link transmission where the diversity branches can be physically located in different base stations, which would make it difficult to use maximal ratio combining or equal gain combining [28]. Hence the larger the number of elements, the better the performance of the selection combining process.

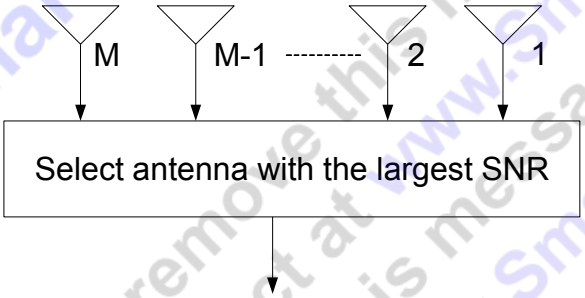

Fig. 2.14 Selection combining.

2.6.3 Equal Gain Combining (EGC)

EGC is a variant of the Maximal Ratio Combining technique. The weights are all set to the same value and are not changed after that. Then the signals are co-phased as in MRC before the summation process. The coherently detected signals from all the branches are simply added and applied to the decision device. As the receiver does not need to estimate the amplitude fading, its complexity is reduced as compared with that of maximal ratio combining [28].

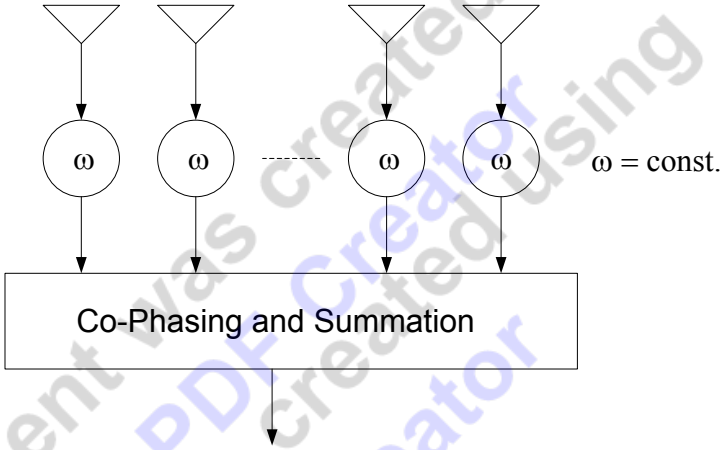

Figure 2.15 Equal gain combining

2.7 Photodetection Noise

The types of noise encountered in optical communications are mainly shot noise and thermal noise. For FSO systems, the noise from the background radiation can be significant, while in fiber optics communication the background radiation noise is negligible. The various sources of noise in optical communications are discussed below -

2.7.1 Photon fluctuation noise

The only significant noise that affects an ideal photodetector performance is that associated with the quantum nature of light itself, the by-product of which is that the number of photons emitted by a coherent optical source in a given time is never constant. Although for a constant power optical source the mean number of photons generated per second is constant, the actual number

of photons per second follows the Poisson distribution. This results in photon fluctuation or quantum noise.

Within the photodetector, the quantum fluctuation is also important because it dominates over the thermal fluctuations, since $hf > kT$ where h and f are the Planck's constant and radiation frequency respectively while κ and T represent the Boltzmann's constant and temperature. The quantum noise is a shot noise with variance:

$$\sigma_{Qtm}^2 = 2q\langle i \rangle B \tag{2.11}$$

where the bandwidth of the electrical filter that follows the photodetector is represented by B Hz.

2.7.2 Dark current and excess noise

The dark current is the photocurrent generated when no photon is impinging on the photodetector. It is produced by the transition of electrons from the valence to the conduction band due to causes other than photon-induced excitation; its magnitude is closely related to the energy band-gap of the photodetector materials. Large band-gap materials, such as Silicon (Si), Indium phosphide (InP) and Gallium arsenide (GaAs) show very low values of mean dark current $\langle i_d \rangle$, while for Germanium (Ge), the value could be significant when they are operated at room temperature [29]. The dark current consists of diffusion, tunnel, leakage currents and generation-recombination taking place in the space-charge region and is proportional to the volume of the depletion region [29].

Photodetectors that employ internal avalanche gain mechanism to boost the signal above the thermal noise of amplifier stages on the receiver exhibit what is referred to as excess noise [30]. According to [30], the excess noise in an APD is due to the multiplication process in the high-field region of the detector where each primary electron hole can generate an additional electron through impact ionization of bound electrons. These additional carriers can then create still additional carriers in a cascading process. Dark current can also contribute to excess noise. There are two types of dark current that can generate excess noise, surface dark current and bulk dark current. Both types generate primary carriers that are Poisson distributed and therefore add yet another noise process that competes with the signal even without multiplication [30].

2.7.3 Background radiation

This type of noise is due to the detection of photons generated by the environment. Two types of sources contribute to background radiation noise, these are: localized point sources (e.g. the Sun) and extended sources (e.g. the sky). Background radiation from other celestial bodies such as stars and reflected background radiation are assumed to be too weak to be considered for a terrestrial FSO link; however they contribute significantly to background noise in deep space FSO. The following are the irradiance (power per unit area) expressions for both the extended and localized background sources [22][31][32]:

$$I_{sky} = N(\lambda)\Delta\lambda\pi\,\Omega^2/4 \tag{2.12a}$$

$$I_{sun} = W(\lambda)\Delta\lambda \tag{2.12b}$$

where $N(\lambda)$ and $W(\lambda)$ are the spectral radiance of the sky and spectral radiant emittance of the sun, respectively, $\Delta\lambda$ is the bandwidth of the optical band pass filter (OBPF) that precedes the photodetector, and Ω is the photodetector's field of view angle (FOV) in radians. By carefully choosing a receiver with a very narrow FOV and $\Delta\lambda$, the impact of background noise can be greatly reduced. Optical BPF in the form of coatings on the receiver optics/telescope with $\Delta\lambda < 1$ nm are now readily available. Empirical values of $N(\lambda)$ and $W(\lambda)$ under different observation conditions are also available in literature [18][22][32]. The background radiation is a shot noise with variance [22]:

$$\sigma_{Bg}^2 = 2qBR_d(I_{sky} + I_{sun}) \tag{2.13}$$

Combining these noise processes together results in the total shot noise whose variance, σ_{sh}^2, is the sum of the individual noise variances and R_d is the photodetector responsivity . This is however dominated by the background radiation as the other two are usually smaller.

2.7.4 Thermal noise

This is the noise caused by the thermal fluctuation of electrons in any receiver circuit of equivalent resistance R_L, and temperature T. The thermal noise is regarded as a 'white' noise. This is because the power spectral density (PSD) is independent of frequency. Moreover, the thermal noise obeys the Gaussian distribution with mean zero and has a variance defined by [33]:

$$\sigma_{Th}^2 = \frac{4kTB}{R_L} \tag{2.14}$$

where k is the Boltzmann's constant.

2.8 Intensity Modulated Direct Detection (IM/DD) System

In Intensity Modulation, amplitude of the output light varies in accordance with the instantaneous value of the message signal. This modulated light is directly converted into electrical current by a photodiode at the receiver end what is termed as direct detection (DD).Jointly these two processes is intensity modulated direct detection (IM/DD) system. In Fig. 2.16 Simplified block diagram of an optical intensity modulated direct detection communications system is depicted. Most practical wireless optical channels use light emitting diodes or lasers as transmitters and photodiodes as detectors. These devices modulate and detect solely the intensity of the carrier, not its phase, which implies that all transmitted signal intensities are nonnegative.

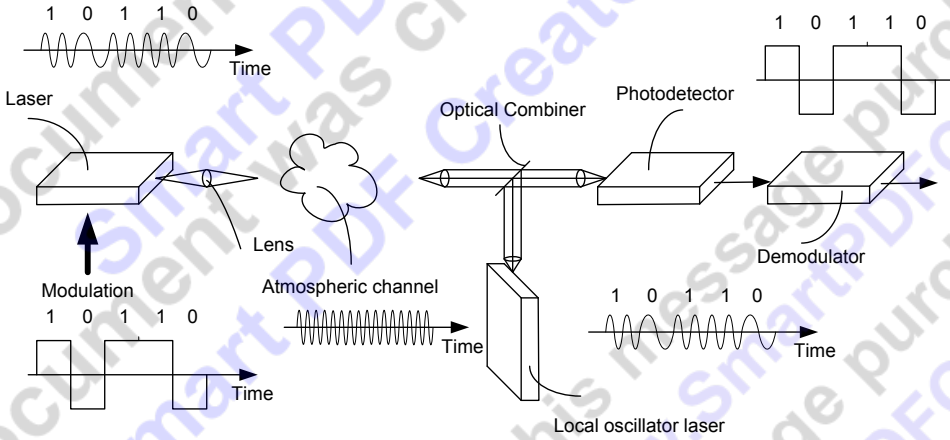

Fig. 2.16 Simplified block diagram of an optical IM/DD communications system.

2.9 Summary

A review of the FSO technology has been carried out in this chapter. Key features that make FSO suitable for use within the access network have been highlighted while the challenges posed by the atmospheric channel to an optical beam travelling through it have also been introduced. The different types of noise also have been discussed in this chapter.

Chapter 3

Analysis of STBC Coded Optical Free Space Link

Chapter-3

Analysis of STBC Coded Optical Free Space Link

3.1 Introduction

The analysis of optical Free Space Link using Alamouti-type Space Time Block Codes is presented in this chapter. Intensity Modulated Direct Detection (IM/DD) system is considered in this thesis. The motivation behind this thesis work is the performance limitation of OOK modulated FSO in atmospheric turbulence channels. Analysis includes the development of the expression of SNR and BER for an FSO Link over weak atmospheric turbulence channel. Analysis is extended to multiple optical receivers with Selection Combining (SC) and Maximal Ratio Combining (MRC).

3.2 Space Time Block Code (STBC) for FSO Links

3.2.1 Alamouti Code [34]

In MIMO technology, space-time block coding is a simple and ingenious transmit diversity technique. Alamouti proposed a simple scheme for a *[2 × 2]* MIMO system that achieves a full diversity gain with a simple maximum likelihood decoding algorithm. It also satisfies for higher-order diversity systems involving a large number of antennas, and whose basic approach is also available in [34].

The information bits are first modulated using an *M*-ary modulation scheme. The encoder then takes a block of two modulated symbols x_1 and x_2 in each encoding operation and gives it to the transmit antennas according to the code matrix,

$$S = \begin{bmatrix} x_1 & -x_2^* \\ x_2 & x_1^* \end{bmatrix} \tag{3.1}$$

In eq. (3.1), the first column represents the first transmission period and the second column the second transmission period. The first row corresponds to the symbols transmitted from the first

antenna and the second row corresponds to the symbols transmitted from the second antenna. During the first symbol period, the first antenna transmits x_1 and the second antenna transmits x_2. In second symbol period, transmits $-x_2^*$ and x_1^* respectively. This implies that symbols are both transmitted in space (across two antennas) and time (two transmission intervals) as shown in fig 3.1.

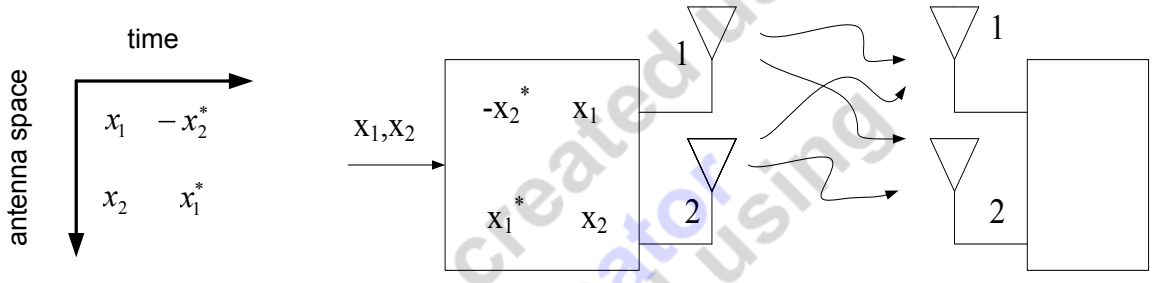

Fig. 3.1 Two transmit two receive Alamouti STBC Block Diagram.

From fig. 3.1

$$s_1 = [x_1 \quad -x_2^*]$$
$$s_2 = [x_2 \quad x_1^*] \tag{3.2}$$

where s_1 is the information sequence from the first antenna and s_2 is the information sequence from the second antenna.

3.2.2 Alamouti-type STBC [35]

Proposed Alamouti STBC was absolutely suitable for complex valued data for microwave MIMO channel. But for FSO communication, data through the optical links are considered to be intensity modulated. That is the reason why complex valued data would not be able to transmit through the FSO channel in the same manner as conventional Alamouti STBC. A new scheme has been proposed by Simon *et al.* [35] considering real valued data only, named after Alamouti as Alamouti-type STBC for FSO channel.

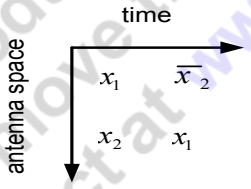

Fig. 3.2 Two transmit two receive Alamouti-type STBC.

where, $x_i = \sqrt{2p_i}$, p_i is the power of i-th symbol.

3.3 System Block Diagram

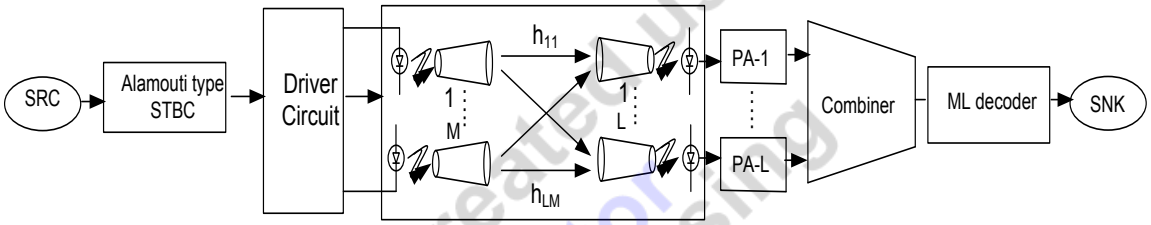

Fig. 3.3 Block diagram representation of the system.

The total system block diagram is shown in fig 3.3. The Alamouti-type STBC coded OOK data is transmitted by the laser sources and received by photodetector using direct detection method. At the receiver end, the incoming optical radiation is passed through an optical band pass filter (OBPF) before being converted into an electrical signal by the photo detector. The OBPF is used to limit the amount of background radiation noise detected by the photodetector. The received signals (photodetectors current) are then passed through the pre-amplifier (PA). The outputs of the pre-amplifiers are then put into the combiner. Various methods such as maximal ratio combiner (MRC), selection combiner (SC), equal gain combiner (EGC) etc have been proposed for combining independently faded signal components and the trade off among these methods is the receiver complexity versus transmission performance improvement. The performance of maximal ratio combiner and selection combiner are compared in this thesis work.

3.4 Theoretical Analysis for SNR & BER

In FSO system, all the signals are the light intensity, they must be real signals. For OOK modulation, the signals can be described as:

$$s_1 = 0 \quad ; \qquad 0 < t \le T_b \text{ light off}$$

$$s_2 = A \quad ; \qquad 0 < t \le T_b \text{ light on}$$

where „A“ is a positive constant related to the intensity of the light source and T_b is the bit duration. We can express one of these signal waveforms in terms of the other by

$$s_i = -s_j + A \quad ; \quad j \neq i \tag{3.3}$$

The new formation of the transmit symbols become as:

$$\{s_1, s_2\} \rightarrow \begin{bmatrix} x_1 & \bar{x}_2 \\ x_2 & x_1 \end{bmatrix}$$

For the FSO system we define the complement of a signal x_i as $\bar{x}_i$ where x_i and $\bar{x}_i$ are used for "light on" and "light off" respectively. For example, if $x_i = s_1$, then

$$\bar{x}_i = s_2 = -s_1 + A = -x_i + A \tag{3.4}$$

Otherwise, if $x_i = s_2$, then $\bar{x}_i = s_1 = -s_2 + A = -x_i + A$

The transmitted optical signal by the lasers are

for laser-1,
$$\begin{aligned} S_1(t) &= \sqrt{2P_s\varepsilon} \qquad for \quad 0 \angle t \angle \frac{T_b}{2} \\ &= -\sqrt{2P_s\varepsilon} + A \quad for \quad \frac{T_b}{2} \angle t \angle T_b \end{aligned} \tag{3.5}$$

for laser-2,
$$\begin{aligned} S_2(t) &= \sqrt{2P_s\varepsilon} \qquad for \quad 0 \angle t \angle \frac{T_b}{2} \\ &= \sqrt{2P_s\varepsilon} \qquad for \quad \frac{T_b}{2} \angle t \angle T_b \end{aligned}$$

where T_b is the bit duration.

At the receiver end, the received photo current for i^{th} photodetector is -

$$i_i(t) = R_d |s_i(t)|^2 \times |h_i|^2 + n(t) = 2R_d P_s \varepsilon |h_i|^2 + n(t) = 2R_d I |h_i|^2 + n(t)$$

The total photodetector"s current is given by

$$i(t) = \begin{bmatrix} |h_{11}|^2 & |h_{21}|^2 \\ |h_{12}|^2 & |h_{22}|^2 \end{bmatrix} \times 2R_d I + n(t) \tag{3.6}$$

$$i_{ji}(t) = \left|h_{ji}\right|^2 \times 2R_d I + n(t)$$

$$i(t) = \sum_{j=1}^{L}\sum_{i=1}^{M} i_{ji}$$

where

R_d = photodetector responsivity

P_s = symbol power (power at the bias level of the semiconductor)

ε = modulation index

I = maximum optical intensity

$n(t)$ = AWGN (Additive White Gaussian Noise)

= Thermal Noise+ Background radiation shot noise

The additive white Gaussian noise $n(t)$ consists of both the thermal noise and the background radiation shot noise.

The shot noise and background noise respectively are given by

$$\sigma^2_{shot} = 2qB.i_{sho} \tag{3.7}$$

$$\sigma^2_{bg} = 2qB_{el}.i_{bg} \tag{3.8}$$

where

B_{el} =Post detection electrical filter bandwidth.

i_{bg} =Background current=$R_d\, I_{bg}$

I_{bg}= background radiation irradiance.

Eq (3.8) can be written as

$$\sigma^2_{bg} = 2qB_{el.}\, R_d\, I_{Bg} \tag{3.9}$$

The thermal noise is given by

$$\sigma^2_{th} = 4kTB_{el} / R_L \tag{3.10}$$

where

k = Boltzman constant = $1.38*10^{-23}$

R_L = Receiver circuit load resistance

T = Temperature

Considering the background noise and thermal noise power from equations (3.9) and (3.10), total noise power becomes

$$\begin{aligned}\sigma^2 &= \sigma^2_{bg} + \sigma^2_{th} \\ &= 2qB_{el.} R_d I_{Bg} + 4kTB_{el}/R_L \\ &= 2 B_{el.}(qR_d I_{Bg} + 2kT/R_L)\end{aligned} \tag{3.11}$$

In presence of turbulence the total bit energy to noise spectral density ratio is expressed as

$$\begin{aligned}\bar{\gamma} &= \bar{h}_{ji}^2 E_b / N_0 \\ &= \bar{h}_{ji}^2 2R_d P_s \varepsilon T_b / N_0 \\ &= \bar{h}_{ji}^2 2R_d P_s \varepsilon / (N_0 \frac{1}{T_b}) \\ &= \bar{h}_{ji}^2 2R_d P_s \varepsilon / \sigma^2\end{aligned} \tag{3.12}$$

In OOK, E_b represent the energy of the detected pulse in the „on" state.

Assuming transmission matrices based on real orthogonal designs for full rate and a full diversity space time block code, the adoption of an array based on M laser sources, all pointed towards a distant array of L photodetectors, implies a diversity of order LM, so that the conditional BER is given by [13]

$$P_b\left(E\left|\{h_{ji}\}_{\substack{1\le i\le M \\ 1\le j\le L}}\right.\right) = Q\left(\sqrt{\frac{E_b}{2N_0}\sum_{j=1}^{L}\sum_{i=1}^{M} h_{ji}^2}\right) \tag{3.13}$$

where $Q(x)$ is the Gaussian-Q function with argument x and $\frac{E_b}{N_o}$ is the total bit energy to noise spectral density ratio in RF literature in the absence of turbulence. In optical literature $\sqrt{\frac{E_b}{N_o}}$ is often defined as SNR.

From Eq. (3.13) using the alternating form of Q(x), is obtained as

$$P_b\left(E\middle|h_{ji}\right)=\frac{1}{\pi}\int_0^{\frac{\pi}{2}}\prod_{j=1}^{L}\prod_{i=1}^{M}\exp\left(-\frac{\bar{\gamma}\,h_{ji}^2}{2\times 2\sin^2\theta}\right)d\theta \tag{3.14}$$

The conditional BER averaged over the pdf of the channel irradiance thus yielding

$$P_b(E)=\underbrace{\int_0^{\infty}\int_0^{\infty}\cdots\quad\cdots\quad\cdots\int_0^{\infty}}_{ML-fold}\frac{1}{\pi}\int_0^{\frac{\pi}{2}}\prod_{j=1}^{L}\prod_{i=1}^{M}\left[\exp\left(-\frac{\bar{\gamma}\,h_{ji}^2}{2\times 2\sin^2\theta}\right)\times p(h_{ji})\right]d\theta\,dh_{11}dh_{12}\cdots\quad\cdots dh_{ji}\cdots dh_{LM} \tag{3.15}$$

where

$$p(h_{ji})=\frac{1}{(2\pi\sigma_X^2)^{0.5}h_{ji}}\exp\left(-\frac{(\log_e h_{ji}-\mu_x)^2}{2\sigma_X^2}\right),\quad a>1 \tag{3.16}$$

where the mean $\mu_x=-\frac{\sigma_x^2}{2}$.

By changing the order of integration in (3.15) and one gets subsequently grouping the terms of index ij,

$$P_b(E)=\frac{1}{\pi}\int_0^{\frac{\pi}{2}}[D(\theta,\bar{\gamma})]^{LM}d\theta \tag{3.17}$$

where

$$D(\theta,\bar{\gamma})=\int_0^{\infty}\exp\left(-\frac{\bar{\gamma}\,h^2}{2\times 2\sin^2\theta}\right)\times\frac{1}{\sqrt{2\pi\sigma_x^2}\,h}\exp\left(-\frac{(\log_e h+\frac{\sigma_x^2}{2})^2}{2\sigma_x^2}\right)dh \tag{3.18}$$

A closed-form solution of (3.18) does not exist and could result in truncating the upper limit using the numerical integration. By using an alternative representation of the Q-function together with the Gauss-Hermite quadrature integration [36], these problems can be circumvented. These are expressed as

$$Q(x) = \frac{1}{\pi}\int_0^{\frac{\pi}{2}} \exp(-\frac{x^2}{2\sin^2\theta})d\theta \tag{3.19}$$

$$\int_{-\infty}^{\infty} f(x)\exp(-x^2)dx \cong \sum_{i=1}^{m} w_i f(x_i) \tag{3.20}$$

where $\{x_i\}_{i=1}^m$ and $\{w_i\}_{i=1}^m$ represent the zeros and weight factors of the mth order Hermite polynomial respectively [37, 38]. The degree of accuracy of (3.20) is determined by the value of m.

Let us consider

$$x = \frac{(\log_e h + \frac{\sigma_x^2}{2})}{\sqrt{2\sigma_x^2}} \tag{3.21}$$

Thus, $h = \exp(\sqrt{2\sigma_x^2}\,x - \frac{\sigma_x^2}{2})$ and $dh = \sqrt{2\sigma_x^2}\,\exp(\sqrt{2\sigma_x^2}\,x - \frac{\sigma_x^2}{2})dx$ (3.22)

Using (3.20), (3.21) and (3.22) in (3.17) the resultant BER is obtained as,

$$P_b(E) = \frac{1}{\pi}\int_0^{\frac{\pi}{2}}\left[\frac{1}{\sqrt{\pi}}\sum_{i=1}^{m} w_i \exp\left(-\frac{\bar{\gamma}\exp(2\sqrt{2\sigma_x^2}\,x_i - \sigma_x^2)}{2\times 2\sin^2\theta}\right)\right]^{ML} d\theta \tag{3.23}$$

3.5 BER Analysis using MRC at the Receiver

The MRC combiner weights each output signal by gain $\{a_i\}_{i=1}^L$ proportional to the received intensity. The optimum combiner output SNR (γ_{MRC}) is given as [36]

$$\gamma_{MRC} = \left(\frac{R_d\varepsilon}{\sqrt{2L}}\right)^2 \sum_{i=1}^{L}\frac{h_i^2}{\sigma^2} = \sum_{i=1}^{L}\gamma_i \tag{3.24}$$

where $\gamma_i = \left(\frac{R_d \varepsilon h_i}{\sqrt{2L\sigma}} \right)^2$ is the SNR for each link, R_d the photodetector responsivity and ε the modulation index considering two laser sources. The joint pdf of scintillation is given by

$$p_{MRC}(h) = \prod_{i=1}^{L} p(h_i) \tag{3.25}$$

Thus, the BER becomes

$$P_{bMRC}(E) = \frac{1}{\pi} \int_0^{\frac{\pi}{2}} [D(\theta, \gamma_{MRC})]^L d\theta \tag{3.26}$$

where

$$D(\theta, \gamma_{MRC}) \approx \frac{1}{\sqrt{\pi}} \sum_{j=1}^{m} w_j \exp\left(-\frac{\gamma_{MRC}}{2\sin^2\theta} \exp\left[2(x_j \sqrt{2\sigma_x^2} - \frac{\sigma_x^2}{2}) \right] \right)$$

3.6 BER Analysis using SC at the Receiver

In this scheme, the combiner selects the link with the highest SNR without the need to estimate the phase. The pdf of the received intensity, $h=max\ (h_1,h_2,\ldots\ldots,h_L)$ is obtained by first obtaining its cumulative density function and then taking the derivative. With the assumption of independent and identical distributed intensity, the pdf is found as [36, 39].

$$p(\max(h_1, h_2 \cdots, h_L)) = \frac{2^{1-L} L \exp(-x^2)}{\sqrt{2\pi\sigma_x^2 h}} \times [1 + erf(x)]^{L-1} \tag{3.27}$$

where $x = \dfrac{(\log_e h + \frac{\sigma_x^2}{2})}{\sqrt{2\sigma_x^2}}$

Now the unconditional BER is obtained [39]

$$P_b(E) = \frac{1}{\pi} \int_0^{\frac{\pi}{2}} \left[\frac{2^{1-L} L}{\sqrt{\pi}} \sum_{i=1}^{m} w_i \times [1 + erf(x_i)]^{L-1} \exp\left(-\frac{\gamma_{SC} \exp(2\sqrt{2\sigma_x^2} x_i - \sigma_x^2)}{2\sin^2\theta} \right) \right] d\theta \tag{3.28}$$

where

$$\gamma_{SC} = \left(\frac{R_d \varepsilon \bar{h}}{\sqrt{2L\sigma}} \right)^2$$

3.7 Simulation of Alamouti-type Coded System

Transmitter Output:

For the FSO system shown in Fig. 3.3, all the signals must be real signals. Based on the above FSO communication model, the received signals in the first and second bit intervals, respectively, are given by

$$\begin{bmatrix} y_1 & y_2 \end{bmatrix} = \begin{bmatrix} h_{11} & h_{12} \end{bmatrix} \begin{bmatrix} x_1 & \bar{x}_2 \\ x_2 & x_1 \end{bmatrix} + \begin{bmatrix} n_1 & n_2 \end{bmatrix} \tag{3.29}$$

where n_1, n_2 are modeled as independent zero-mean Gaussian noise with variance σ^2.

For log-normal case, the amplitude of the random path gain H is $H = e^X$, where X is normal with mean μ_X and variance σ_X^2. Thus, the logarithm of the field amplitude scale factor is normally distributed. The optical intensity $I = H^2$ is also log normally distributed in this case. The probability density function for H is given by Eq. (2.3)

If we designate the total incident power (spatial integral of the field intensity) at one photodetector as P_r watts, the effective K count parameter of the Poisson count variable is

$$n_s = \frac{\eta P_r T}{hf} = \frac{\eta E_s}{hf} \text{ photoelectrons/slot.}$$

and the effective count parameter due to the background field denoted as n_b. This is related to the total incident background power on one photodetector P_b by

$$n_b = \frac{\eta P_b T}{hf} = \frac{\eta E_b}{hf} \text{ photoelectrons/slot.}$$

However, the fading does not affect the background radiation, by assumption. Hence, the count parameter for the ℓ th detector in the "on" slot, conditioned on a set of fading variables $H_{\ell m} = a_{\ell m} \equiv h_{\ell m}$, is $n_s \sum_{m=1}^{M} a_{\ell m}^2 / M + n_b$, where n_b is defined as above in the absence of fading. For strong turbulent model the optical irradiance, $I_{\ell m} \equiv h_{\ell m}$. The division by M accounts for the power sharing among M lasers, in order that the total laser array's power is constant [12].

Receiver Output:

Assuming the channel gains and the transmitted signal power are known, the receiver uses the sequence that can be written as [35]:

$$\left.\begin{aligned} \tilde{x}_1 &= h_{11} y_1 + h_{12} y_2 - h_{11} h_{12} A \\ \tilde{x}_2 &= h_{12} y_1 - h_{11} y_2 + h_{11}^2 A \end{aligned}\right\} \tag{3.30}$$

However, from eqs. (3.3) , (3.4) and (3.29), $\bar{s}_2 = -s_2 + A$ Using this in Eq. (3.30) gives

$$\left.\begin{aligned} \tilde{x}_1 &= (h_{11}^2 + h_{12}^2) x_1 + h_{11} n_1 + h_{12} n_2 = (h_{11}^2 + h_{12}^2) x_1 + \tilde{N}_1 \\ \tilde{x}_2 &= (h_{11}^2 + h_{12}^2) x_2 + h_{12} n_1 - h_{11} n_2 = (h_{11}^2 + h_{12}^2) x_2 + \tilde{N}_2 \end{aligned}\right\} \tag{3.31}$$

This is the set of decision metrics identical to those in the conventional Alamouti code. Where the noise samples $\tilde{N}_1$ and $\tilde{N}_2$ are uncorrelated and since they are complex Gaussian, they are also independent [35]. Thus, the modified Alamouti code as described above produces a diversity of order *2*.

Suppose now that the system contains L photodetectors. As such, the generalization of Eq. (3.29) becomes

$$\left.\begin{aligned} y_\ell &= h_{\ell 1} x_1 + h_{\ell 2} x_2 + n_\ell \\ y_{\ell+L} &= h_{\ell 1} \bar{x}_2 + h_{\ell 2} x_1 + n_{\ell+L} \end{aligned}\right\} \quad \ell = 1, 2, \cdots, L \tag{3.32}$$

where $y_\ell, \ell = 1,2,3,\cdots,L,$represents the signals received by the *L*-th photodetector in the first bit interval and $y_{\ell+L}, \ell = 1,2,3,\cdots,L$, represents the signals received by the *L*-th photodetector in the second bit interval corresponding to a single transmission of the Alamouti code. At the receiver, we now form [analogous to Eq. 3.30] the decision statistics as:

$$\tilde{x}_1 = \sum_{\ell=1}^{L_r} h_{\ell 1} y_\ell + \sum_{\ell=1}^{L_r} h_{\ell 2} y_{\ell+L_r} - A \sum_{\ell=1}^{L_r} h_{\ell 1} h_{\ell 2}$$

$$\tilde{x}_2 = \sum_{\ell=1}^{L_r} h_{\ell 2} y_{\ell} + \sum_{\ell=1}^{L_r} h_{\ell 1} y_{\ell+L_r} + A \sum_{\ell=1}^{L_r} h_{\ell 1}^2 \tag{3.33}$$

The Maximum-Likelihood Decision:

For the receiver, we usually use the ML decision rule to get the source code, assume the receive signal vector is y= (y1, y2), so we can define the formulation of the ML decision as [35]:

$$\begin{aligned} m\,(y,x) &= [y_1 - (h_{11}x_1 + h_{12}x_2)]^2 + [y_2 - (h_{11}\bar{x}_2 + h_{12}x_1)]^2 \\ &= y_1^2 + y_2^2 - 2[(h_{11}y_1 + h_{12}y_2)x_1] - 2[(h_{12}y_1 - h_{11}y_2)x_2] \\ &\quad - 2[h_{11}y_2(\bar{x}_2 + x_2)] + (h_{11}^2 + h_{12}^2)x_1^2 + (h_{11}^2 + h_{12}^2)x_2^2 \\ &\quad + h_{11}^2(\bar{x}_2^2 - x_2^2) + 2[h_{11}h_{12}x_1(\bar{x}_2 + x_2)] \end{aligned} \tag{3.34}$$

Using (3.30), this can be written as

$$\begin{aligned} m\,(y,x) &= y_1^2 + y_2^2 - 2[(\tilde{x}_1 + h_{11}h_{12}A)x_1] - 2[(\tilde{x}_2 - h_{11}^2 A)x_2] \\ &\quad - 2(h_{11}y_2 A) + (h_{11}^2 + h_{12}^2)x_1^2 + (h_{11}^2 + h_{12}^2)x_2^2 \\ &\quad + h_{11}^2(A^2 - 2Ax_2) + 2(h_{11}h_{12}x_1 A) \\ &= y_1^2 + y_2^2 - 2\tilde{x}_1 x_1 - 2\tilde{x}_2 x_2 - 2(h_{11}y_2 A) \\ &\quad + (h_{11}^2 + h_{12}^2)(x_1^2 + x_2^2) + h_{11}^2 A^2 \\ &= y_1^2 + y_2^2 - \tilde{x}_1^2 - \tilde{x}_2^2 + (\tilde{x}_1 - x_1)^2 + (\tilde{x}_2 - x_2)^2 \\ &\quad - 2(h_{11}y_2 A) + (h_{11}^2 + h_{12}^2 - 1)(x_1^2 + x_2^2) + h_{11}^2 A^2 \end{aligned} \tag{3.35}$$

Eliminating terms from Eq. (3.35) that are hypothesis-independent, then for the purpose of decision making the metric simplifies to

$$\begin{aligned} m(\tilde{x}, x) &= (\tilde{x}_1 - x_1)^2 + (h_{11}^2 + h_{12}^2 - 1)\, x_1^2 \\ &\quad + (\tilde{x}_2 - x_2)^2 + (h_{11}^2 + h_{12}^2 - 1)\, x_2^2 \end{aligned} \tag{3.36}$$

which is identical to that for the conventional Alamouti code. Finally, since the pair of information signals x_1 and x_2 to be transmitted is independently chosen from the binary signal alphabet, then an ML decision can be made separately on each of them using the metric

$$m(\tilde{x}_i, x_i) = (\tilde{x}_i - x_i)^2 + (h_{11}^2 + h_{12}^2 - 1)x_i^2, \quad i = 1,2 \tag{3.37}$$

with the corresponding decision rule:
Choose $x_i = \hat{x}_i$ iff

$$(\tilde{x}_i - \hat{x}_i)^2 + (h_{11}^2 + h_{12}^2 - 1)\hat{x}_i^2 \le (\tilde{x}_i - x_i)^2 + (h_{11}^2 + h_{12}^2 - 1)x_i^2 \tag{3.38}$$

for $x_i \neq \hat{x}_i$

3.8 Summary

In this chapter theoretical analysis on FSO MIMO communication system based on Alamouti-type STBC with intensity modulation direct detection with different combining techniques at the receiver has been discussed. The performance analysis has been done in terms of bit error rate (BER).

Chapter 4

Results and Discussion

Chapter-4

Results and Discussion

4.1 Introduction

In this chapter, the BER performance of an IM/DD optical FS link without STBC over log normal turbulence channel is evaluated numerically. For STBC coded FSO system, we carry out the simulation considering OOK modulation over the log normal turbulence model. Results are evaluated in terms of BER as a function of average SNR without and with STBC considering weak turbulence model.

4.2 Results and Discussion

In this thesis the performance of FSO communication through atmospheric channel using Alamouti-type STBC has been analyzed. The performance for Alamouti-type STBC coded optical FS link with optical intensity modulation and direct detection in the presence of atmospheric turbulence is observed. When the length of a FSO medium such as air is increased, then the effect of atmospheric turbulence will be significant. Log-normal Model has been used to represent the atmospheric effect during weak turbulence.

First the BER has been observed varying different parameters for a double transmitter and single detector. Then for multiple detectors, the BER has been presented and it is clearly found that the performance is considerably improved i.e. the BER is significantly decreased for added photodetectors diversity.

The numerical computation and graphical representation have been done by using MATLAB software throughout this chapter. Different parameters used for computation in this chapter are shown in the following table-

Table 4.1 Nominal parameters used in FSO communication link

Parameter Name	Value
Bit Rate	1 Gbps
Modulation Index	1.0
Responsivity of the Detector	0.85
Modulation	OOK
Channel Type	Log-normal
Turbulence Varience	0.1 to $\angle 1.2$
Load resistance	50Ω
Temperature	300K
Coding	Alamouti-type STBC
Radiation wavelength	1550 nm
Average receiver power of one PD, P_r	10^{-8} w
Average background radiation power of one PD, P_b	10^{-10} w
Mean irradiance, I_o	1
Bandwidth	0.25 × Bit Rate
Plank's constant, h	6.63×10^{-34}
Electron's charge, q	1.6×10^{-19} c

4.2.1 Observation of BER of a FSO Link with two Transmitters and variable Receivers over log-normal turbulence model with Alamouti-type STBC

Fig. 4.1 shows BER vs. SNR (dB) with two transmitters and one receiver considering turbulence variance 1.0. The BER falls down significantly with increasing SNR for Alamouti-type STBC over log-normal turbulence model.

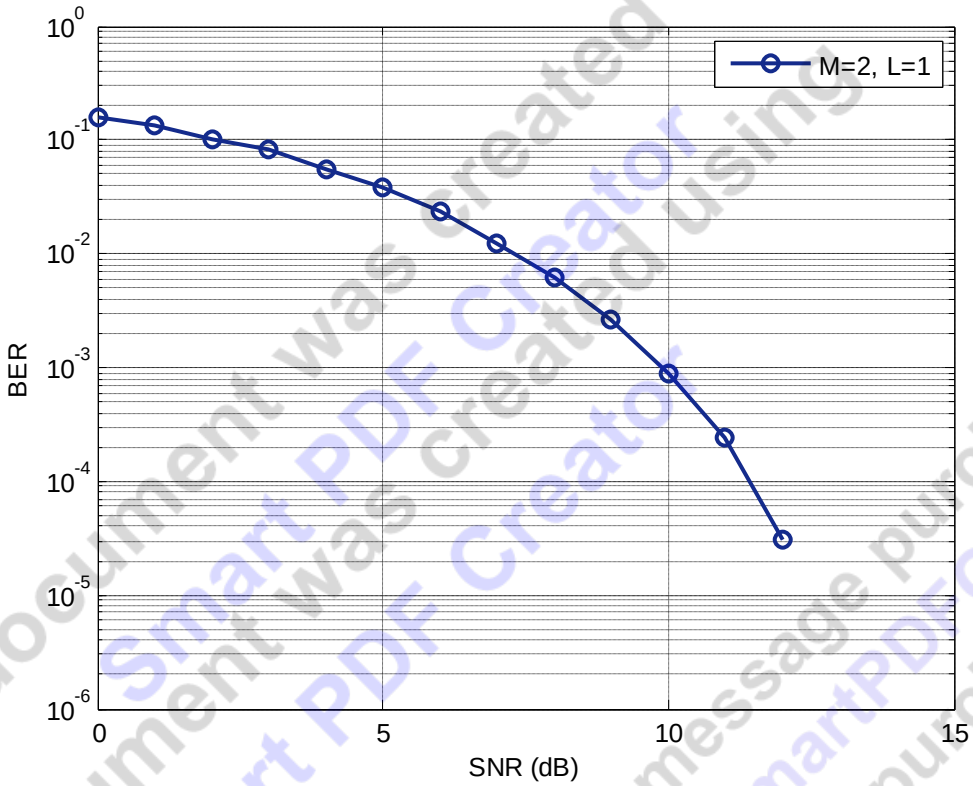

Fig. 4.1 BER performance of an FSO link over log-normal turbulence model with Alamouti-type STBC.

The same system has been extended for increasing receiver diversity for the same number of transmitters. The improvement of the BER is shown in Fig. 4.2 for this added diversity. At a BER of 10^{-6}, 2×2-MIMO system requires ~2dB additional SNR when compared with 2×4-MIMO system. While for the BER 2×1-MIMO system requires ~5dB additional SNR when compared with 2×4-MIMO system.

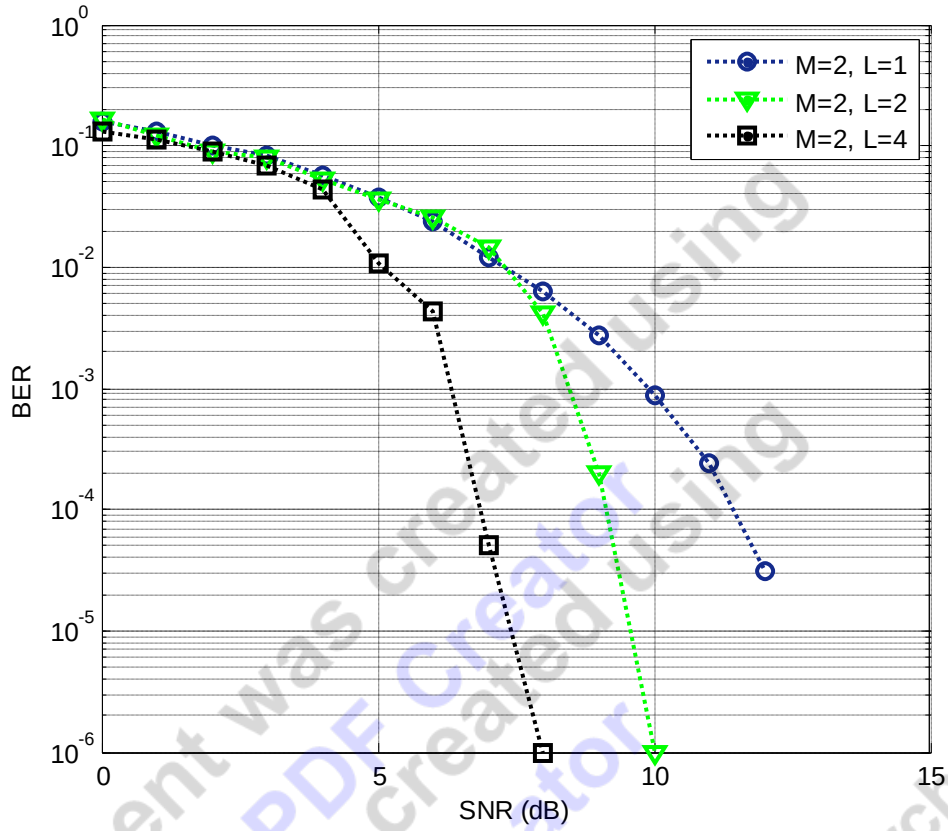

Fig. 4.2 Simulated BER performance of an FSO link over log-normal turbulence model with Alamouti-type STBC with different receiver diversity.

Table 4.2 Link margin (diversity gain) at BER of 10^{-6}

MIMO configuration	2×1	2×2	2×4
Link margin (dB)	~13	~10	~8

4.2.2 Observation of BER of a FSO Link with two Transmitters and variable Receivers using analytical expression

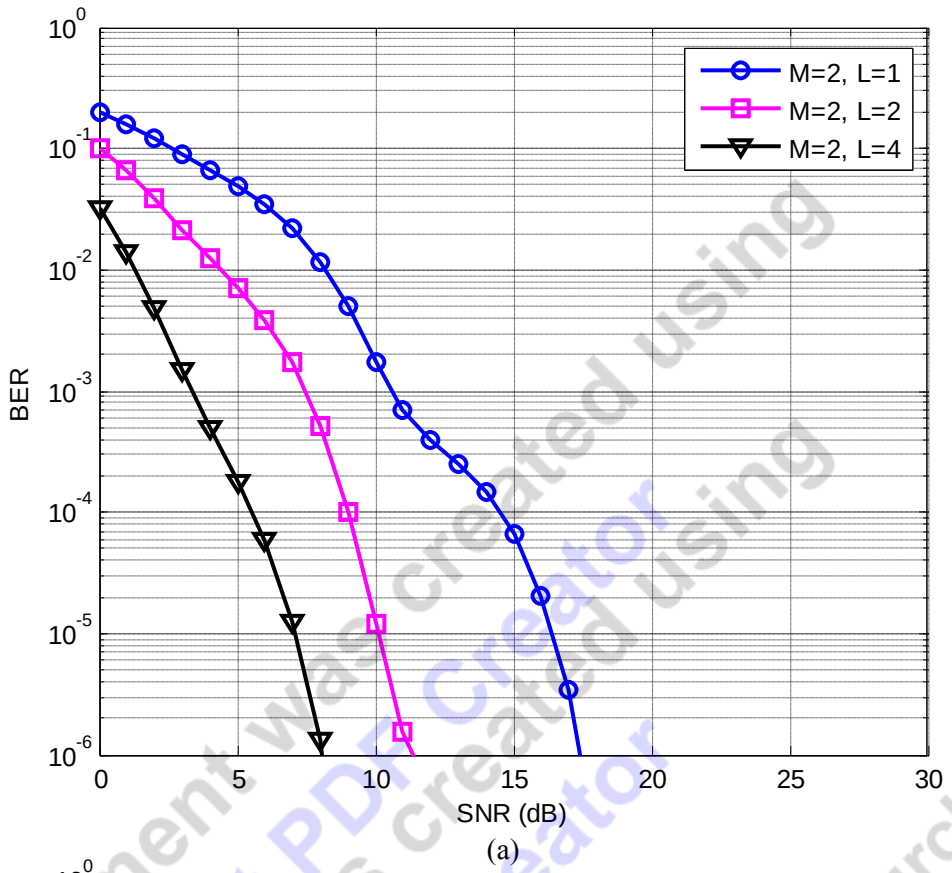

(a)

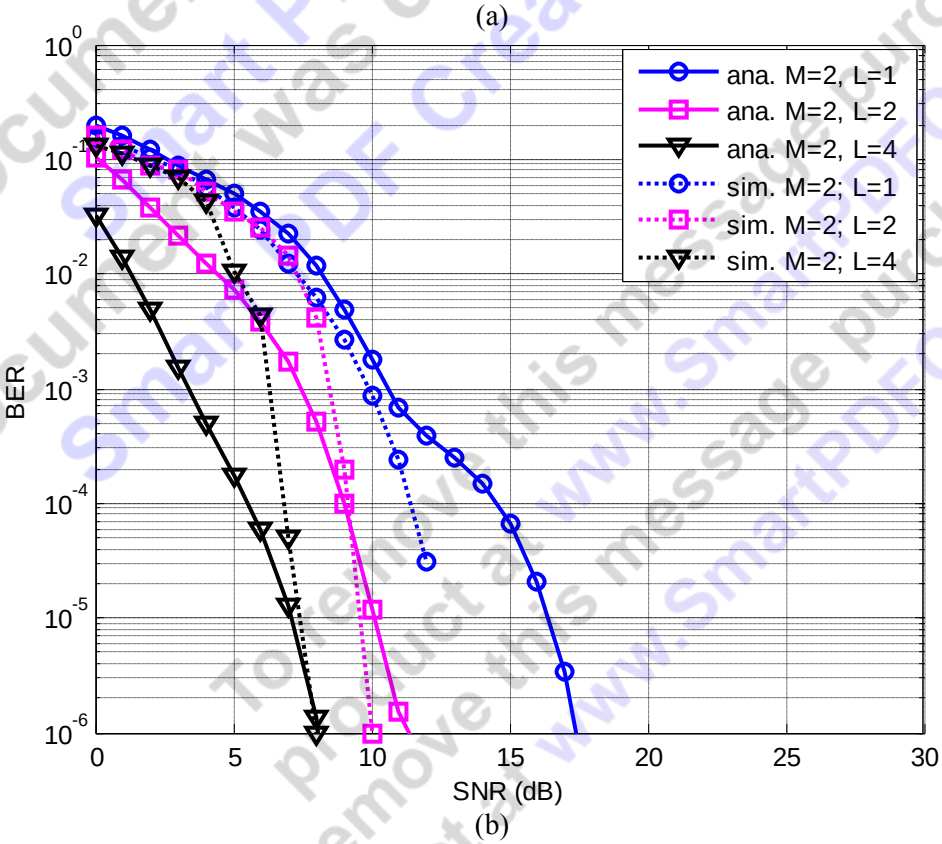

(b)

Fig. 4.3 Analytical and Simulated BER performance of an FSO link over log-normal turbulence model with Alamouti-type STBC with different receiver diversity.

Fig. 4.3 (a) and (b) shows the analytical and simulated BER performance of an FSO link over log-normal turbulence model with Alamouti-type STBC with different receiver diversity respectively. Both analytical and simulated results are nearly same.

4.2.3 Observation of BER of a FSO Link with two Transmitters and variable Receivers over log-normal turbulence model with and without Alamouti-type STBC

Fig. 4.4 shows BER curve for both with & without Alamouti type STBC at weak atmospheric turbulent condition. Both analytical and simulated results are presented in the same graph.

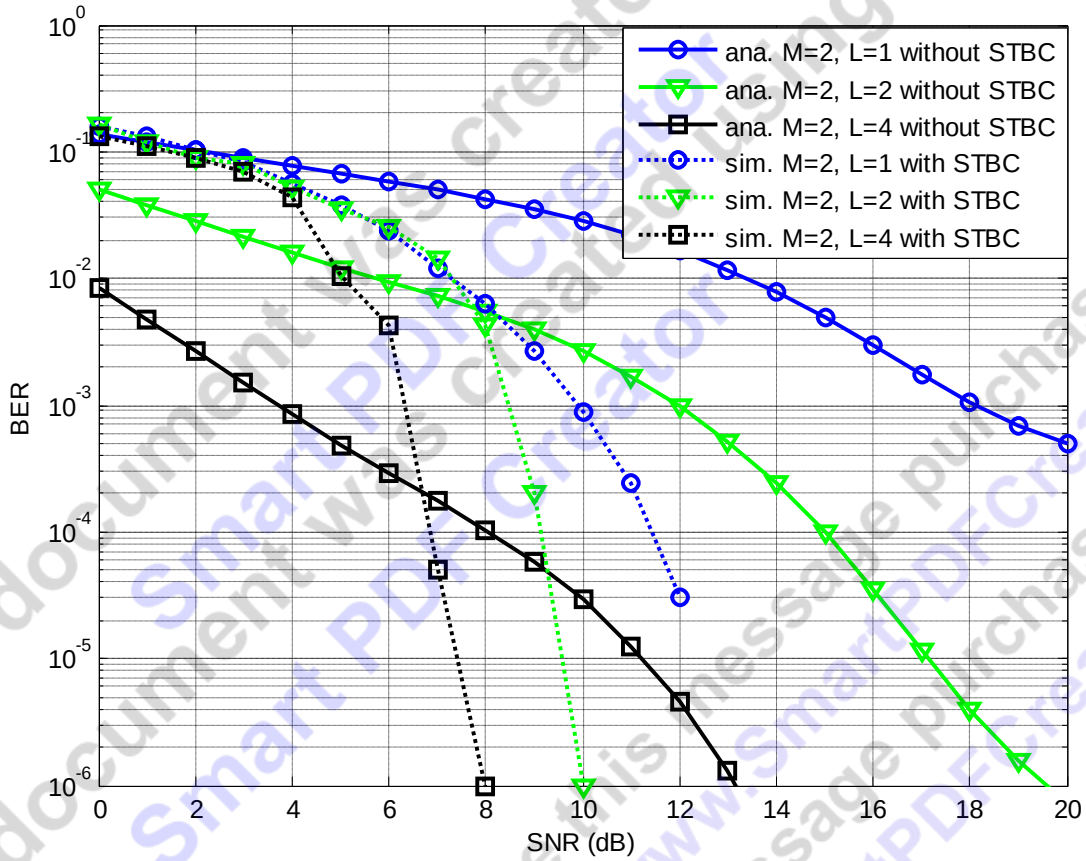

Fig. 4.4 BER curves for both with and without STBC over weak atmospheric turbulent condition for analytical and simulated results.

Table 4.3 Link margin (diversity gain) at BER of 10^{-6}

MIMO configuration		2×1	2×2	2×4
Link margin (dB)	With STBC	~13	~10	~8
	Without STBC	~31	~19.7	~13

Eqn. 10 [21] is used for without STBC. It is observed from Table 4.3 that without STBC dB requirement is more than that of with STBC. As an example, two laser sources, all pointed towards a distant array of *L = 1, 2, 4* photodetectors, is considered. Simulation results only up to $BER = 10^{-6}$ are included, which demonstrate an excellent agreement with the analytical results. It is noticed that there are significant improvement in receiver sensitivity due to receive diversity without and with STBC. The MRC diversity at a $BER = 10^{-6}$ with or without STBC for weak turbulence (*M = 2, L = 1, 2, 4*) the SNR improvement due to diversity is found to be ~ *18dB, ~ 10 dB, ~5dB* respectively.

4.2.4 Observation of BER of a FSO Link with two Transmitters and variable Receivers for both weak and strong atmospheric turbulent condition with Alamouti-type STBC

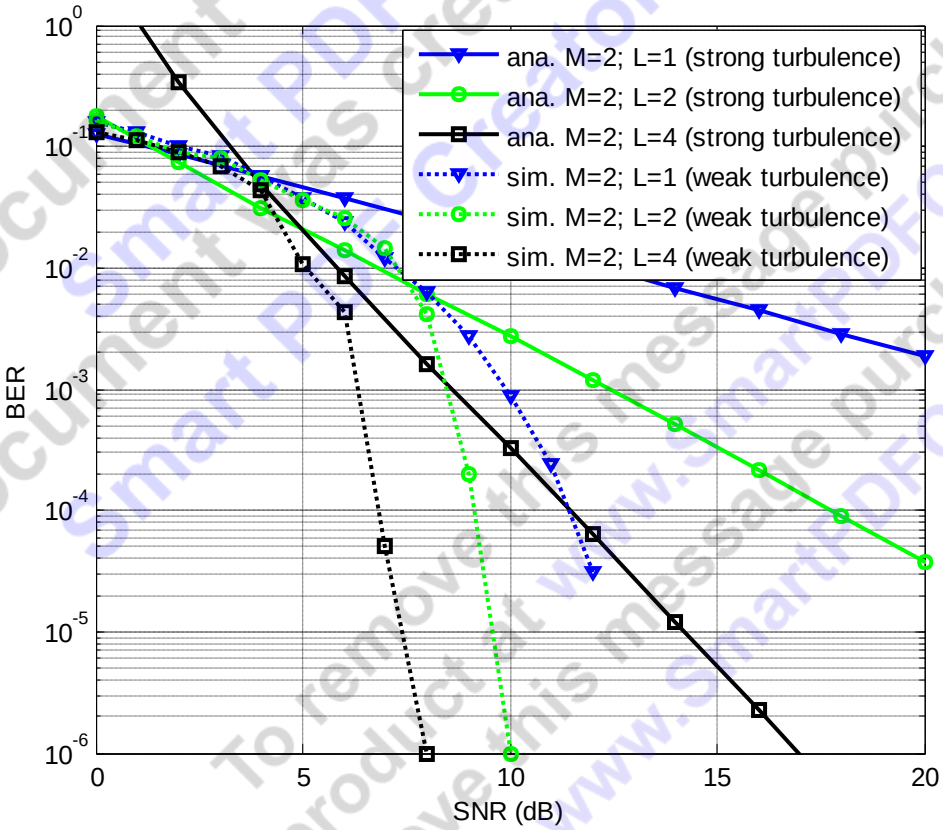

Fig. 4.5 BER curve for Alamouti type STBC in both weak & strong atmospheric turbulent condition for analytical and simulated results.

Fig. 4.5 represents the BER performance for Alamouti-type STBC for both weak and strong atmospheric condition. Eqn. 14 [13] is used for strong atmospheric turbulence with Alamouti-type STBC. The analytical and simulated results are also presented together. It evident from the figure that under weak and strong turbulence (*M = 2, L =1, 2, 4*) the SNR improvement is found to be ~ *27dB, ~16 dB* and ~ *9 dB* respectively for Alamouti type STBC. The numerical values are presented in Table 4.4.

Table 4.4 Link margin (diversity gain) at BER of 10^{-6}

MIMO configuration		2×1	2×2	2×4
Link margin (dB)	Strong turbulence	~40	~26	~17
	Weak turbulence	~13	~10	~8

4.2.5 Observation of Sensitivity Improvement due to Receiver Diversity

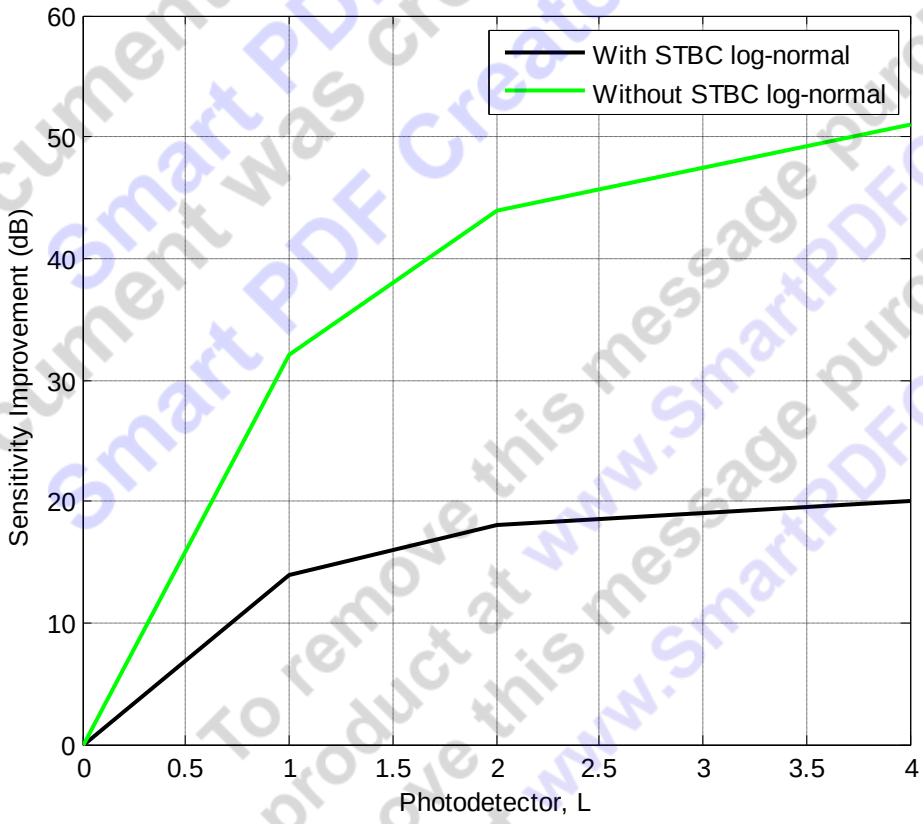

Fig. 4.6 Sensitivity improvement curve due to receiver diversity for both with & without STBC over log normal turbulent condition.

The receiver sensitivity increases with addition of more number of detectors. It is revealed from Fig. 4.6 that the receiver sensitivity improvement is better for without STBC than with STBC over log-normal channel. The plots of improvement in receiver sensitivity are shown in figure 4.6 at a $BER = 10^{-6}$.

4.3 Observation of BER of a FSO Link with two Transmitters and variable Receivers over log-normal atmospheric turbulent condition with different combining techniques at the receiver.

4.3.1 Maximal Ratio Combining (MRC)

Fig. 4.7 shows the BER vs. SNR of an FSO system with two transmitters and one receiver over log-normal channel using maximal ratio combiner at the receiver. The BER is observed under different turbulent variance condition. The SNR requirement increases almost at a linear rate for the turbulent variance less than 50%. It increases slowly as variance increases as shown in Table 4.5.

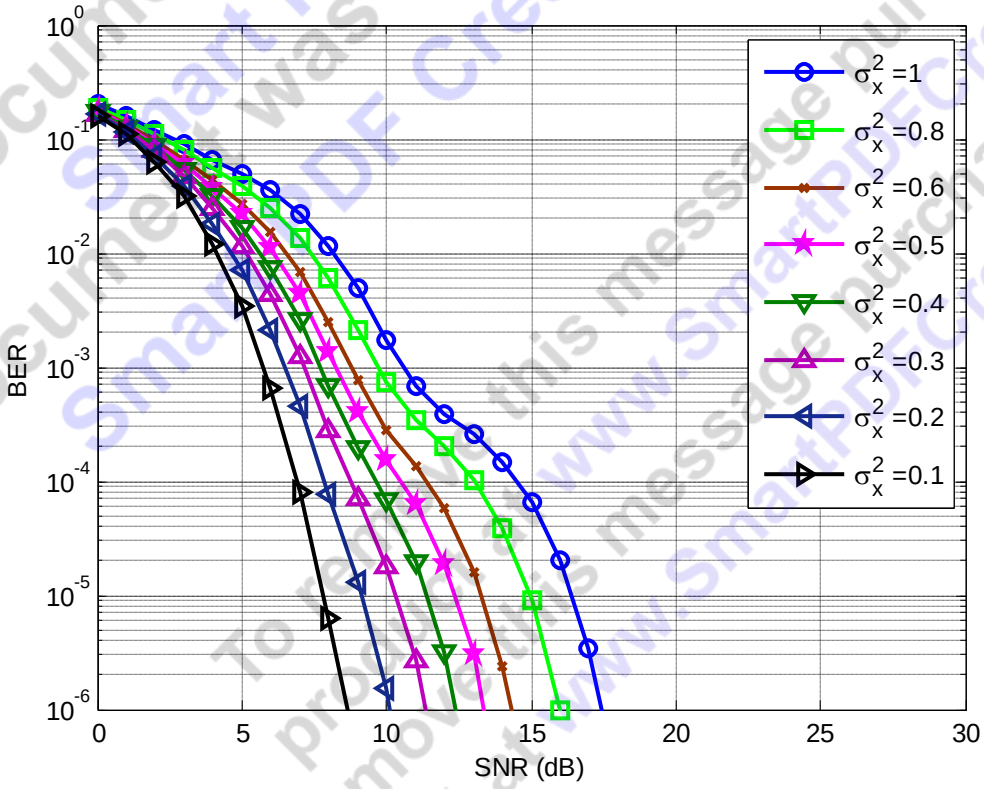

Fig. 4.7 BER performance curve for FSO link over log-normal turbulent condition with varying turbulence variance considering M=2, L=1 and MRC at the receiver.

Table 4.5 Required SNR for different tubulence variance at BER of 10^{-6}

Variance (σ_x^2)	0.1	0.2	0.3	0.4	0.5	0.6	0.8	1
Required SNR (dB)	~8.2	~10	~11.4	~12.5	~13.5	~14.3	~16.1	~17.3

The observation in Fig. 4.7 is extended with added diversity keeping fixed variance. It is obvious that with added diversity BER decreases significantly as shown in Fig. 4.8. The approximate summary of the BERs are presented in Table 4.6. ~8.8 dB saving of SNR can be achieved with 2×8 in compared with 2×1 MIMO system. So the performance of the system can improved with increment of possible link budget.

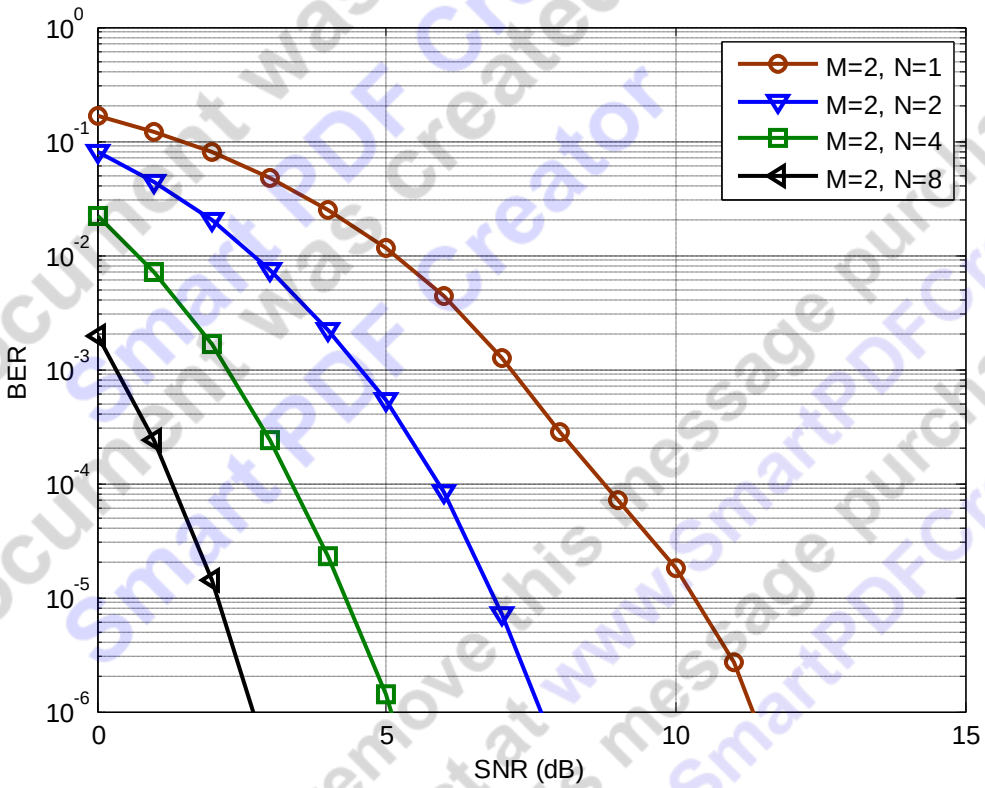

Fig. 4.8 BER performance curve for FSO log-normal with different detector diversity at a variance = 0.3 using MRC Combining at receiver.

Table 4.6 Required SNR for MIMO for variance 0.3 at a BER of 10^{-6}

MIMO configuration	2×1	2×2	2×4	2×8
Required SNR (dB)	~11.8	~7.8	~5.1	~3

The BER is investigated further for varying variance for different added diversity, shown in Fig. 4.9. It is already found from Fig. 4.8 that added diversity results in less SNR requirement for an FSO link for log-normal channel. The similar thing also happens for less variance as well, shown in Fig. 4.7. But in comparison with these two scenarios added diversity shows better performance than varying turbulence variance condition.

The summary of the last two simulated results is shown in Table 4.7 for better understanding at a glance.

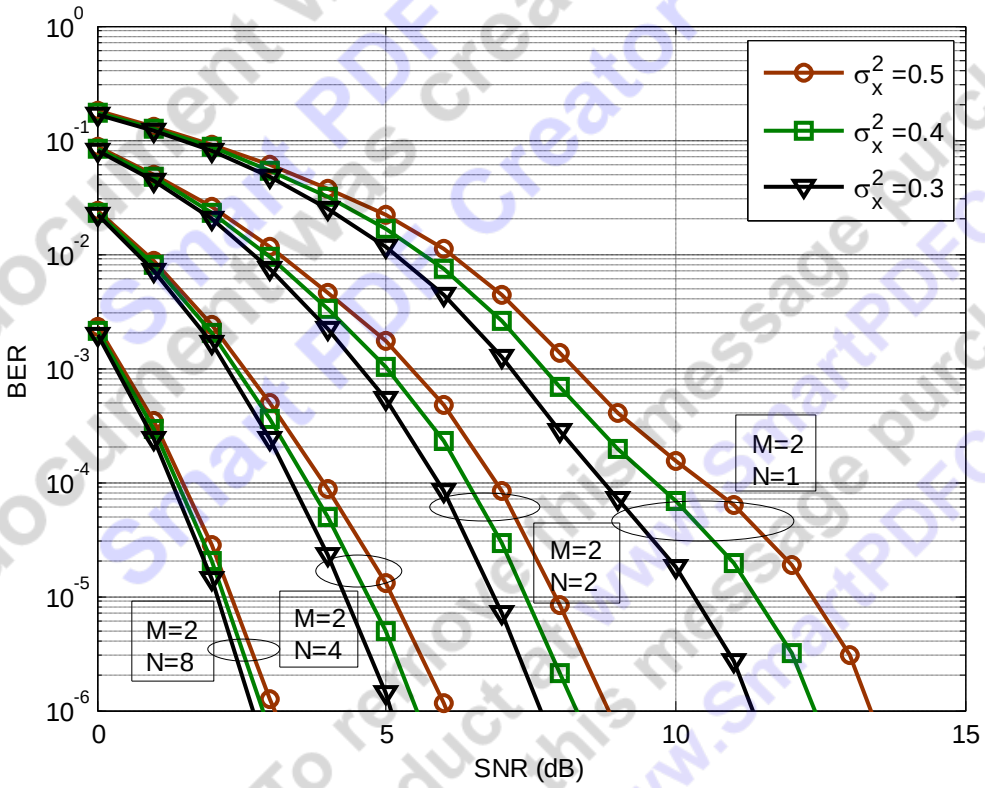

Fig. 4.9 BER performance curve for FSO log-normal with different detector diversity with different variance using MRC at the receiver.

Fig. 4.9 shows the BER curves for log-normal channel under different MIMO configurations with varying turbulence variance. Four set of BER curves are simulated for different scenarios.

The more the diversity added the more the BER decreases. For 2×1 configuration ≤~1dB improvement is obtained while for 2×2 and 2×4 configurations ≤~0.5dB and for 2×8 configurations ≤~0.2dB is obtained for varying variances. Under different MIMO configurations the trade off BER is very much significant which is revealed in table 4.7. For 2×8, 2×4 and 2×2 detectors ~4dB, ~3dB and ~2dB savings could be achieved with compared to single detector 2×1 respectively.

Table 4.7 Required SNR for MIMO for varying variance at a BER of 10^{-6}

MIMO configuration		2×1	2×2	2×4	2×8
Required SNR (dB)	Variance (σ_x^2=0.3)	~11.8	~7.8	~5.1	~3
	Variance (σ_x^2=0.4)	~12.5	~8.4	~5.6	~3.2
	Variance (σ_x^2=0.5)	~13.2	~8.9	~6.1	~3.4

4.3.2 Selection Combining (SC)

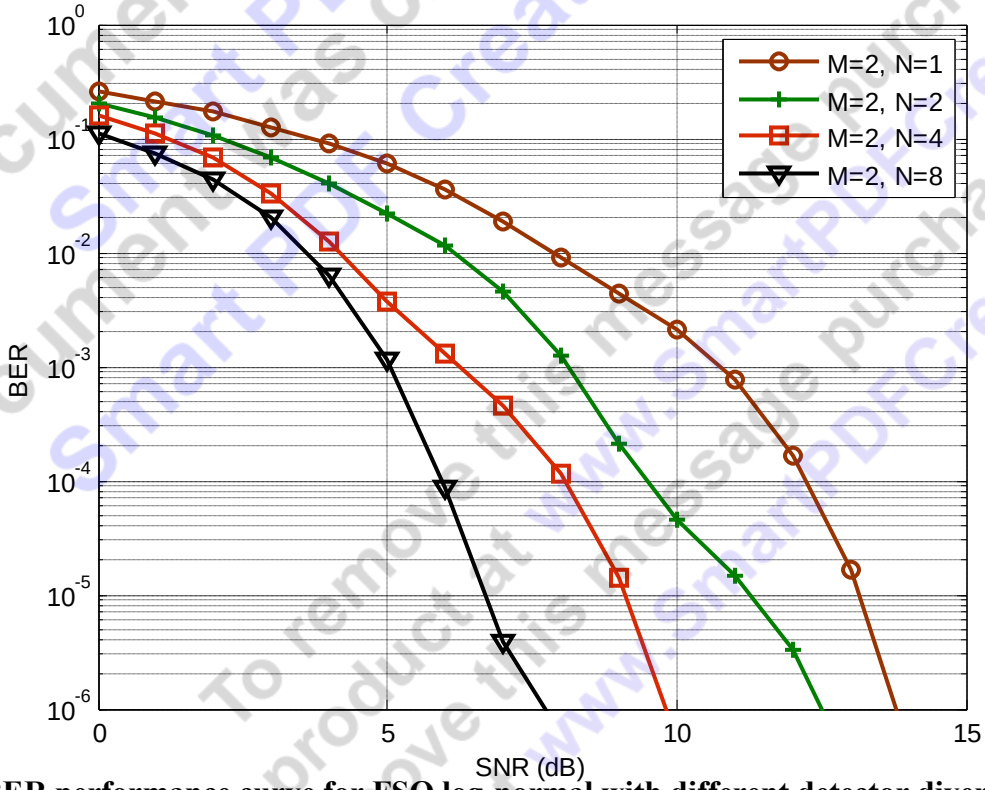

Fig. 4.10 BER performance curve for FSO log-normal with different detector diversity at a variance = 0.3 using Selection Combining at the receiver.

For different MIMO configurations with turbulent variance 0.3, the BER performance curves are plotted against SNR in Fig 4.10 under log-normal channel considering Selection Combining technique at the receiver. The simulated approximate numerical results are in tabular for better comparative study beneath Table 4.8. Here with increase in diversity the BER also decreases. The simulated results are unlike MRC technique with respect to BER performance trade off. The savings of SNR is nearly ~6.1dB, ~4dB and ~1.3dB for 2×8, 2×4 and 2×2 MIMO configurations with respect to 2×1 MIMO configuration respectively.

Table 4.8 Required SNR for MIMO for variance 0.3 at a BER of 10^{-6}

MIMO configuration	2×1	2×2	2×4	2×8
Required SNR (dB)	~13.8	~12.5	~9.8	~7.7

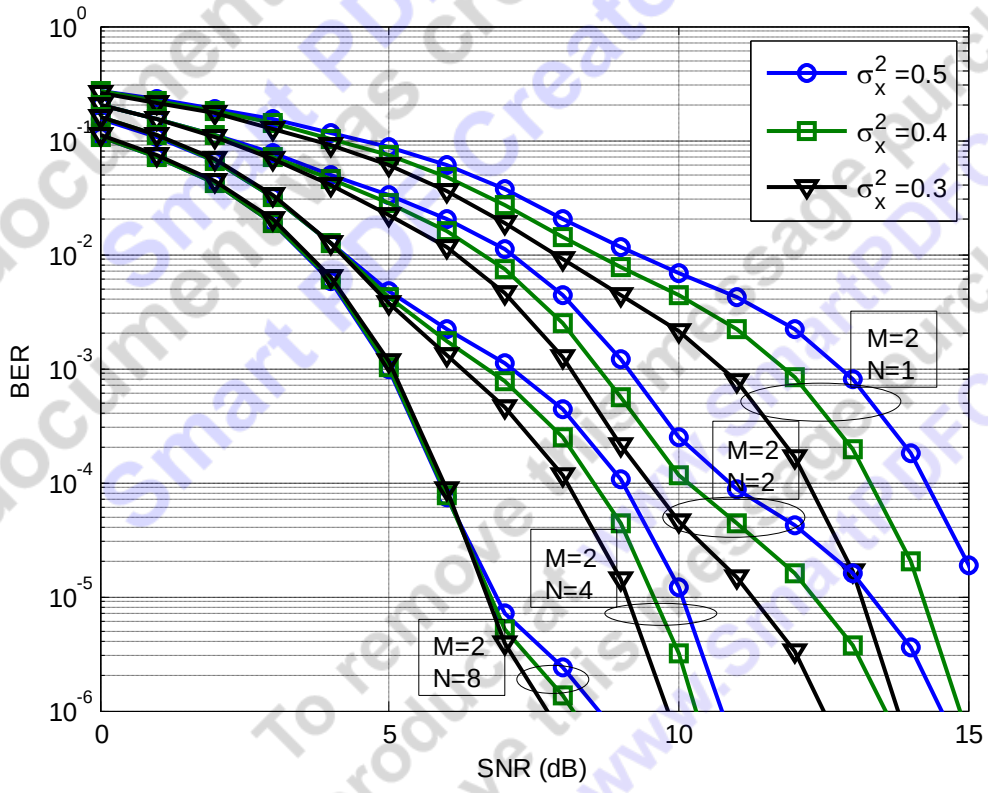

Fig. 4.11 BER performance curve for FSO log-normal with different detector diversity with different variance using SC at the receiver.

Fig. 4.11 shows the BER curves for log-normal channel under different MIMO configurations with varying turbulence variance using selection combining at the receiver. Four set of BER curves are simulated for different scenarios.

4.3.3 Comparison between Maximal Ratio Combining and Selection Combining

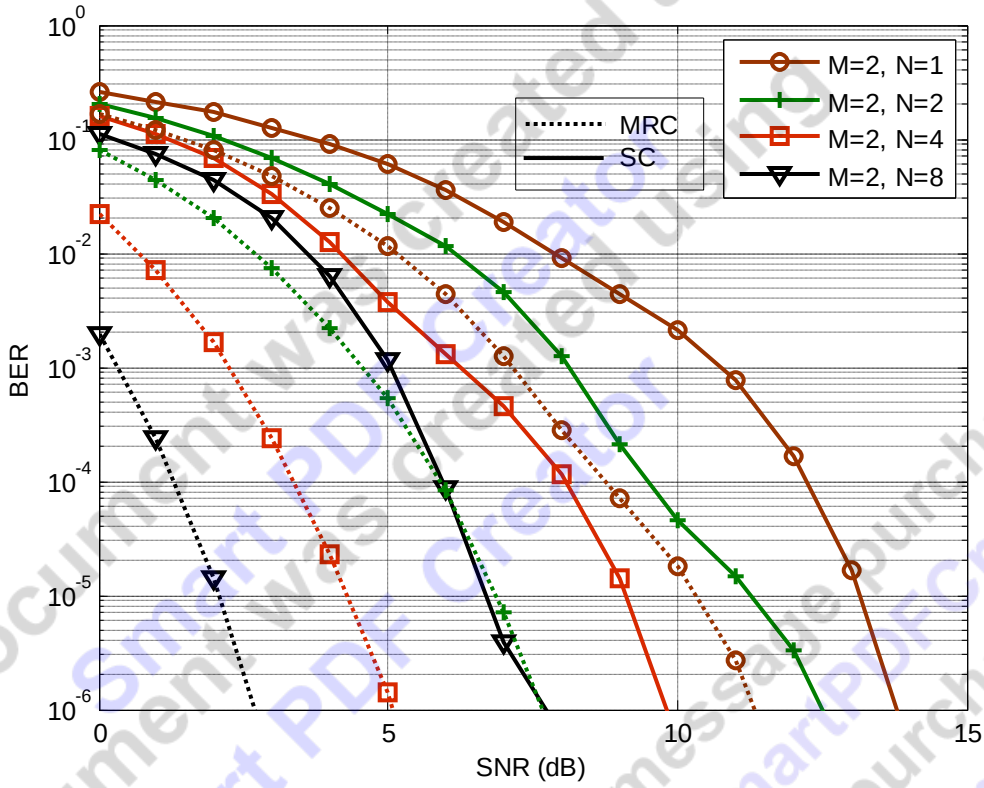

Fig. 4.12 BER performance comparison curve for FSO log-normal with different detector diversity at a variance = 0.3 using both MRC and SC at the receiver.

Fig. 4.12 shows the BER performance of different MIMO configuration considering both MRC and SC at the receiver over log-normal channel. These two receiver combining techniques are depicted together for comparative study of their performance analysis. Numerical values of SNRs are presented in Table 4.9 at BER 10^{-6}. The noise variance is kept constant for both the cases (variance = 0.3). The performance of MRC is much better than that of SC. The savings of SNR is nearly ~4.7dB, ~4.7dB, ~4.7dB and ~2dB for 2×8, 2×4, 2×2 and 2×1 MIMO configurations respectively.

Table 4.9 Required SNR for FSO log-normal with different detector diversity at a variance = 0.3 using both MRC and SC at the receiver at a BER of 10^{-6}

MIMO configuration		2×1	2×2	2×4	2×8
Link margin (dB)	MRC	~11.8	~7.8	~5.1	~3
	SC	~13.8	~12.5	~9.8	~7.7

The receiver sensitivity increases with addition of more number of detectors. It is revealed from Fig. 4.13 that the receiver sensitivity improvement is better for MRC than SC over log-normal channel. The plots of improvement in receiver sensitivity are shown in figure 4.13 at a $BER = 10^{-6}$.

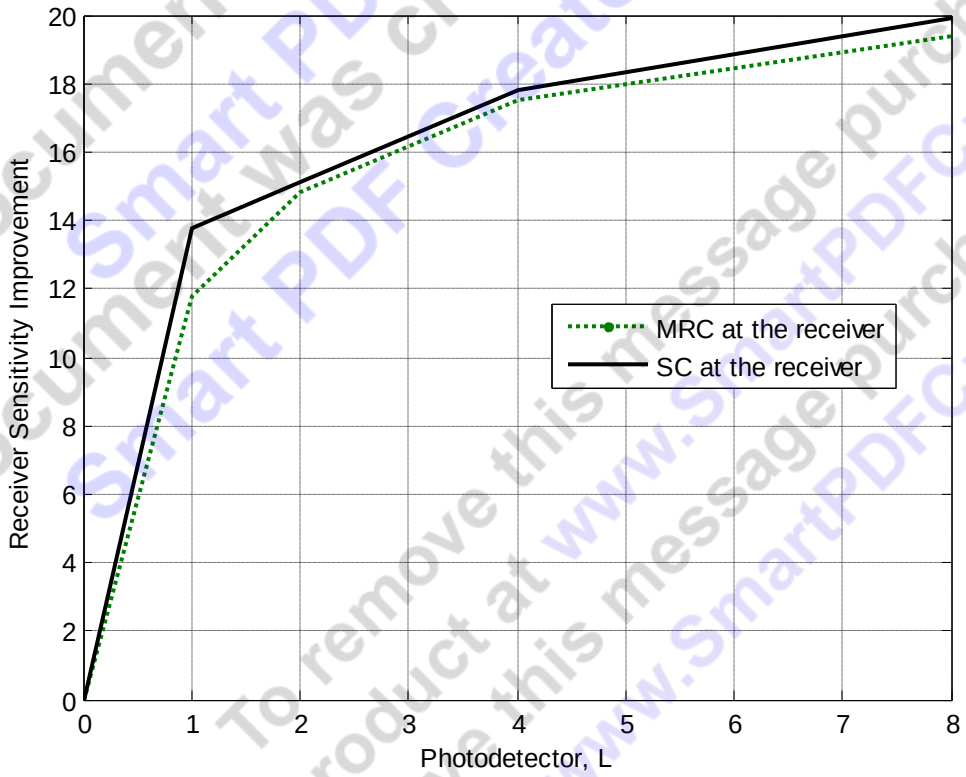

Fig. 4.13 Sensitivity improvement curve due to receiver diversity for both MRC and SC at the receiver over log normal turbulent condition.

4.4 Summary

In this chapter analytical and simulation results are presented in the graphical and tabular format considering atmospheric turbulence. Log-normal model has been considered to represent the weak atmospheric turbulence. From the overall analysis it is clearly found that BER performance is much better for a MIMO system.

Chapter 5

Conclusion and Future Work

Chapter-5

Conclusion and Future Work

5.1 Conclusion

Free space optical (FSO) communication is a very promising technology for the future optical communication networks. But the performance of the free space optical systems can be severely limited by atmospheric effects like fog, rain, smoke etc. The motivation behind this thesis work is the performance limitation of OOK modulated FSO in atmospheric turbulence channels. So, in this thesis the performance of the FSO system is evaluated in the presence of atmospheric turbulence for a MIMO configuration in terms of BER for several parameters.

A turbulent atmospheric channel causes the intensity of an optical beam travelling through it to fluctuate randomly due to random changes in refractive index along the beam's path. In Chapter two, this atmospheric turbulence induced signal fluctuation was reviewed and three most reported models (log-normal, Gamma-gamma and negative exponential) were described and their respective pdfs presented. These models were later used to model the statistical behavior of the received signal for short to very long range FSO systems. Moreover in the FSO communication system, increasing the length of the transmission path is also very much challenging due to the impact of strong atmospheric turbulence. The different types of noise encountered during optical detection were discussed with the view to understanding the limit imposed on the system performance by each of them. The review work revealed that the transmitted photons obey the Poisson distribution and this can be adequately approximated as the tractable Gaussian distribution for large photoelectron counts as is the case in terrestrial FSO systems.

For free space optical transmission systems, most frequently used system is Intensity Modulated Direct Detection (IM/DD) system. In such system, the intensity of an optical source is modulated to transmit signals. For FSO systems, although the power efficiency is inferior to PPM, OOK encoding is more commonly used due to its efficient bandwidth usage and robustness to timing errors. Therefore, in this research work, for FSO systems we prefer intensity modulation/direct detection (IM/DD) with an OOK technique.

The error rate performance for STBC in FSO communication systems with direct detection operating over weak atmospheric turbulence channels is analyzed in this paper. We have simulated the performance of an optical link using Alamouti type space–time block coding at weak and strong atmospheric turbulent condition considering different receiver diversity and also compare the BER curves. In this thesis, it is clearly found that Alamouti-type STBC code can significantly improve the BER performance of FSO system with OOK technique considering weak atmospheric turbulent condition.

5.2 Scope of Future Research Work

- In the free space optical communication, the length of communication channel is very much limited due to atmospheric turbulence in different atmospheric conditions. Still lots of research works should be carried out to increase the length of FSO channel.
- This research work can be carried out by using Space Wavelength Division Multiplexing Block Coding (SWDMBC).
- Work can also be initiated using Pulse Position Modulation instead of OOK modulation.
- FSO with WDM/DWDM can be investigated without and with STBC codes.
- Effect of cloud and other impairments of the atmosphere can be considered in analysis of the FSO Link.

References

[1]. D. Killinger, "Free space optics for laser communication through the air," Optics & Photonics News, vol. 13, pp. 36-42, Oct. 2002.

[2]. A. G. Bell, "On the production and reproduction of sound by light," American Journal of Sciences, vol. Series 3, pp. 305 - 324, Oct. 1880.

[3]. F. E. Goodwin, "A review of operational laser communication systems," Proceedings of IEEE, vol. 58, pp. 1746-1752, Oct. 1970.

[4]. H. Hemmati, "Interplanetary laser communications," Optics and Photonics News, vol. 18, pp. 22-27, Nov. 2007.

[5]. S. Hardy, "Free-space optics systems are finding their niches," Lightwave, pp. 33-36, Dec. 2005.

[6]. I. Kim, "10 G FSO systems position technology for the future," Lightwave online, pp. 19-21, July 2009.

[7]. S. Arnon, "Optimization of Urban Optical Wireless Communication Systems". IEEE Transactions on Wireless Communications, Vol. 4, No. 2, pp 626-629, 2003.

[8]. V. W. S. Chan,"Free-Space Optical Communications" IEEE, Fellow, OSA Journal of Lightwave Technology, Vol. 24, No. 12, pp - 4750-4762, December 2006.

[9]. W. Huang, J. Takayagi, T. Sakanaka and M. Nakagawa; "Atmospheric Optical Communication system Using Subcarrier PSK Modulation," IEEE International Conference, Vol. 3, pp. 1597-1601, May 1993.

[10]. W. G. Stephen.,B. Maïté., C. Qianling, and H. James, " Optical Repetition MIMO Transmission With Multipulse PPM" IEEE journal on selected areas in communications, Vol. 23, No. 9, pp. 1901-1910, September, 2005.

[11]. X. Zhu and J. M. Kahn, "Free-space optical communication through atmospheric turbulence channels", IEEE Transactions on Communications, Vol. 50, pp. 1293-1300, Aug. 2002.

[12]. W. G. Stephen.,B. Maïté., C. Qianling, and H. James, "Free-Space Optical MIMO Transmission with Q-ary PPM". IEEE Trans. on Communications, Vol. 53, No. 8, pp 1402-1412, August 2005.

[13]. G. Z. Antonio, "Error Rate Performance for STBC in Free-Space Optical Communications through Strong Atmospheric Turbulence", IEEE Comm. Letters, Vol. 11, No. 5, pp- 390-392, May 2007.

[14]. S. V. Chinta, T. P. Kurzweg, D. S. Pfeil, K. R. Dandekar; "4 X 4 space – time codes for free space optical interconnects", Photonics Packaging, Integration, and Interconnects . Proceedings of the SPIE, Vol. 7221, pp.722116-722116-8, 2009, DOI: 10.1117/12.809506.

[15]. T. A. Bhuiyan, M. Z. Hassan, S. M. S. Tanzil, S. Hayder, S. P. Majumder, "Performance Improvement of IM-DD Free Space Optical CDMA (Attenuated by Strong Atmospheric Turbulence) with Maximal Ratio Combining", CICN '10 Proceedings of the 2010 International Conference on Computational Intelligence and Communication Networks IEEE Computer Society Washington, DC, USA, 2010, ISBN: 978-0-7695-4254-6, DOI-10.1109/CICN.2010.141

[16]. http://www.electronics-tutorials.ws/diode/diode_8.html

[17]. http://www.mellesgriot.com

[18]. R. M. Gagliardi and S. Karp, Optical Communications, 2nd ed. New York: John Wiley, 1995.

[19]. H. Willebrand, B. S. Ghuman, "Free Space Optics: Enabling Optical Connectivity in Today"s Networks", 2002.

[20]. http://www.severewx.com/Radiation/scattering.html

[21]. W. O. Popoola and Z. Ghassemlooy, "BPSK Subcarrier Intensity Modulated Free-Space Optical Communications in Atmospheric Turbulence," Journal of Lightwave Technology, Vol. 27, No. 8, pp. 967-973, April 15, 2009.

[22]. W. K. Pratt, Laser Communication Systems, 1st ed. New York: John Wiley & Sons, Inc., 1969.

[23]. L. C. Andrews, R. L. Phillips, and C. Y. Hopen, Laser beam scintillation with applications. Bellingham: SPIE, 2001.

[24]. S. F. Clifford, "The classical theory of wave propagation in a turbulent medium," in Laser Beam Propagation in the Atmosphere, J. W. Strobehn, Ed.: Springer-Verlag, 1978.

[25]. E. Bayaki, R. Schober, R. K. Mallik," Performance Analysis of Free-Space Optical Systems in Gamma-Gamma Fading", Global Telecommunications Conference, 2008. IEEE GLOBECOM 2008, DOI:10.1109/GLOCOM.2008.ECP.548, Nov. 30 2008-Dec. 4 2008.

[26]. Z. Hajjarian, J. Fadlullah, and M. Kavehrad, "MIMO Free Space Optical Communications in Turbid and Turbulent Atmosphere "*Journal of Communications*, Vol. 4, No. 8,pp. 524-532, Sep 2009, doi:10.4304/jcm.4.8.524-532.

[27]. P. D. Teal, T. D. Abhayapala, and R. A. Kennedy, "Spatial correlation for general distributions of scatterers," IEEE Sig. Proc. Lett., vol. 9, No.10, pp. 305–308, October 2002.

[28]. J. W. Mark and W. Zhuang , "Wireless communication and Networking"; ISBN-978-81-203-2746-7.

[29]. S. Betti, G. De marchis, and E. Iannone, Coherent Optical Communication Systems, 1st ed. Canada: John Wiley and Sons Inc., 1995.

[30]. G. R. Osche, Optical Detection Theory for Laser Applications. New Jersey: Wiley, 2002.

[31]. S. Karp, E. L. O'Neill and R. M. Gagliardi, "Communication theory for the free-space optical channel", Proceedings of the IEEE, vol. 58, pp. 1626-1650, 1970.

[32]. N. S. Kopeika and J. Bordogna, "Background noise in optical communication systems," Proceedings of the IEEE, vol. 58, pp. 1571-1577, 1970.

[33]. G. Keiser, Optical Communications Essentials 1st ed. New York: McGraw-Hill Professional, 2003.

[34]. S. M Alamouti, "A Simple Transmit Diversity Technique for Wireless Communications", IEEE Journal on select area in Communications, Vol.16, No.8, pp. 1451-1458, October 1998.

[35]. M. Simon and V. Vilnrotter, "Alamouti-type space-time coding for freespace optical communication with direct detection," IEEE Trans. Wireless Commun., vol. 4, no. 1, pp. 35–39, 2005.

[36]. W. O. Popoola, Z. Ghassemlooy, J. I. H. Allen, E. Leitgeb, and S. Gao, "Free-space optical communication employing subcarrier modulation and spatial diversity in atmospheric turbulence channel," IET Optoelectronic, vol. 2, pp. 16-23, 2008.

[37]. M. K. Simon and M. S. Alouini; „Digital communication over fading channels" (John Wiley & Sons Inc., 2004, 2nd edn.)

[38]. M. Abramowitz, and I. S. Stegun, „Handbook of mathematical functions with formulars, graphs and mathematical tables" (Dover,1977).

[39]. Z. Ghassemlooy, W. O. Popoola, V. Ahmadi and E. Leitgeb, "MIMO Free-Space Optical Communication Employing Subcarrier Intensity Modulation in Atmospheric Turbulence

Channels", Communications Infrastructure. Systems and Applications in Europe, Vol. 16. ISBN 978-3-642-11283-6. Springer-Verlag Berlin Heidelberg, pp.61-74, 2009, DOI: 10.1007/978-3-642-11284-3_7.